The Proteasome Inhibitor Bortezomib Induces Tongue, Pharynx and Salivary Gland Cancer Cells Death in Vitro and Delays Tumor Growth of Salivary Gland Cancer Cells Transplanted in Mice

Monica Benvenuto
Saint Camillus International University of Health and Medical Sciences
Sara Ciuffa
University of Rome “Tor Vergata”
Chiara Focaccetti
San Raffaele University Rome
Diego Sbardella
IRCCS-Fondazione G.B. BIETTI
Sara Fazi
University of Rome “Sapienza”
Grazia Raffaella Tundo
University of Rome “Tor Vergata”
Giovanni Barillari
University of Rome “Tor Vergata”
Maria Segni
University of Rome “Sapienza”
Vittorio Manzari
University of Rome “Tor Vergata”
Andrea Modesti
University of Rome “Tor Vergata”
Laura Masuelli
University of Rome “Sapienza”
Massimo Coletta
University of Rome “Tor Vergata”
Roberto Bei (bei@med.uniroma2.it)
University of Rome “Tor Vergata”

Research Article

Keywords: BALB-neuT, SALTO-5, BALB-neuT, HNC, Bortezomib in vivo, transduction pathways proteins

Posted Date: June 1st, 2021

DOI: https://doi.org/10.21203/rs.3.rs-561856/v1

Abstract

Head and neck cancer (HNC) has frequently an aggressive course for the development of resistance to standard chemotherapy. Thus, the use of innovative therapeutic drugs is being assessed. Bortezomib is a proteasome inhibitor with strong in vitro and in vivo anticancer effects. *In vitro* antitumoral activity of Bortezomib was investigated employing human pharynx (FaDu), tongue (SCC-15, CAL-27), salivary gland (A-253) cancer cell lines and a murine cell line (SALTO-5) originated from a salivary gland adenocarcinoma arising in BALB-*neu*T male mice transgenic for the oncogene neu. Bortezomib *in vivo* effects in BALB-*neu*T mice transplanted with murine SALTO-5 cells were also examined. Bortezomib inhibited cells proliferation, triggered apoptosis, modulated the expression and activation of pro-survival signal transduction pathways proteins activated by ErbB receptors and inhibited proteasome activity *in vitro*. Furthermore, intraperitoneal administration of Bortezomib delayed tumor growth of SALTO-5 cells transplanted in BALB-*neu*T mice and protracted mice survival. Our findings further support the use of Bortezomib for the treatment of HNC and reveal its ineffectiveness in counteracting the activation of deregulated specific signaling pathways in HNC cell lines when resistance to proteasome inhibition is developed.

Introduction

Head and neck cancer (HNC) is the seventh leading cause of cancer-related morbidity and mortality, with 890000 new cases diagnosed every year[1,2]. HNC involves several anatomical sites including pharynx, larynx, oral cavity, tongue and salivary glands[2] and often has an aggressive course with emerging resistance to conventional chemotherapy. Salivary gland carcinomas represent 6–8% of HNC, with heterogeneous morphologies and clinical outcomes[3]. The development of new targeted therapies has opened new scenarios for the treatment of solid malignancies[4,5]. Therefore, use of new therapeutic agents is being evaluated in HNC as well[6–9]. Current targeted regimen for HNC patients employs epidermal growth factor receptor (EGFR) inhibitor(s) and the monoclonal antibody cetuximab[1,10]. However, despite promising outcomes in preclinical studies, resistance to anti-EGFR targeted therapies in clinical settings represents a limitation for prolonged use of these drugs[7,11,12].

Among different targeted therapies, inhibitors of the Ubiquitin Proteasome System (UPS), and in particular of the proteasome, are assuming particular importance[13]. They have become a new relevant class of drugs for treatment of tumors, regulation of the immune response and as anti-inflammatory agents[14,15].

The UPS is a major intracellular proteolytic pathway[16]. The substrate, usually early-lived proteins, is conjugated to a chain of at least four ubiquitin (Ub) moieties by E1-E2-E3 enzymes and then delivered to the proteasome, a multi-catalytic assembly, for its enzymatic processing[17]. In the canonical structural configuration, the proteasome is made up by the 19S RP (i.e., Regulatory Particle) which carries out the recognition of poly-ubiquitinated substrates (poly-Ub) and couples their ATP-dependent unfolding with

the translocation into the catalytic chamber of the 20S CP (i.e., Core Particle)[15,17]. Thereafter, the substrate is digested through three enzymatic activities (i.e., chymotrypsin-like, trypsin-like and caspase-like, housed by the β5, β2 and β1 subunits, respectively)[18]. Mature 20S and 19S particles can assemble into different structural configurations, which display an emerging metabolic relevance since they are thought to deal with clearance of different subsets of natural substrates; in particular, poly-ubiquitinated proteins are fed to capped assemblies, whereas oxidized, misfolded or natively unfolded proteins are cleared by the 20S CP[17,19]. Nonetheless, the 20S/capped assemblies ratio has been uncovered to be finely tuned depending on the metabolic need of the cell and every living cell displays proteasome assemblies in the most suited configuration to cope with the maintenance of the proteostasis network (PN). PN defines the equilibrium between protein synthesis and degradation which must be kept unaltered over the cell life cycle to guarantee cell viability and proliferation. Given the central relevance of the UPS in regulating this key network, several pharmacological strategies have been undertaken over the last decades to design drugs which specifically target proteasome proteolytic activity. The purpose of proteasome inhibition is to block the degradation of altered proteins performed by this complex, stimulating the formation of a toxic environment which ultimately triggers the apoptotic processes. As a matter of fact, the use of proteasome inhibitors (PI) in oncology is constantly gaining more interest, as emphasized by the development of next generation proteasome inhibitors. Some of them has already entered clinical trials also in solid malignancies providing outstanding outcomes in terms of overall survival (OS)[15]. In this framework, the clinical success of Bortezomib in treatment of haematological disorders, in particular multiple myeloma, has pioneristically validated the relevance of this therapeutic strategy. Bortezomib is a dipeptidyl boronic acid reversible inhibitor of the chymotrypsin-like activity of the 20S proteasome[14,20,21]. Bortezomib was first synthesized in 1995 and subsequently approved in 2003 as a preferential treatment of multiple myeloma[22]. Bortezomib has been reported to show a potent anticancer activity, both *in vitro* and *in vivo*, also in other cancer cell lines, like prostate cancer, pancreatic cancer, renal cell carcinoma and squamous cell carcinoma[23–26]. In addition, several clinical trials evaluated the effect of Bortezomib in combination with chemotherapy or other targeted therapies in HNC[27–34].

The aim of our research was to evaluate the *in vitro* and *in vivo* antitumoral activity of Bortezomib in HNC. We analyzed the *in vitro* effects of Bortezomib on cells proliferation, cells death, cells cycle regulation, apoptosis, autophagy, expression, and activation of several proteins involved in pro-survival signaling pathways in human and mouse HNC cell lines, including salivary gland cancer cell lines. We also evaluated the effects of Bortezomib in inhibiting the proteasome activity in individual HNC cell lines and correlated for the first time this effect with the modulation of different signal transduction pathways involved in head and neck neoplastic transformation. In addition, we explored for the first time the *in vivo* effects of Bortezomib in mice transplanted with murine adenocarcinoma salivary gland SALTO-5 cell line. Our study therefore provides additional information on the antitumoral effect of Bortezomib and on the development of resistance mechanisms associated with the activation of deregulated specific signaling pathways in HNC cell lines.

Materials And Methods

Reagents

DMSO and Sulforhodamine B (SRB) were purchased from Sigma-Aldrich (Milan, Italy). Bortezomib was purchased from Selleck Chemical (Munich, Germany). Z-VAD-FMK was obtained from Calbiochem (San Diego, CA, USA). Antibodies against Bax, Bcl-2, AKT, phospho-AKT, JNK/SAPK1, JNK/SAPK (pT183/pY185), p38a/SAPK2a, and p38 MAPK (pT180/pY182) were obtained from BD Pharmingen (BD Biosciences, San Jose, CA, USA). Antibodies against caspase 9, caspase 8, activated caspase 3, were obtained from Cell Signaling Technology (MA, United States). Antibodies against PARP-1 (F-2), ERK1/2 (C-14) and phospho-ERK (E-4) were obtained from Santa Cruz Biotechnology (CA, USA). Anti-ErbB2 and anti-EGFR antisera were provided by Dr. M. H. Kraus (University of Alabama, Birmingham, AL, USA). Antibodies against Beclin-1 and p62/SQSTM1 were obtained from Abcam (Cambridge, United Kingdom) and the anti-LC3 antibody was purchased from Novus Biologicals (Littleton, CO, USA). Rabbit polyclonal anti-actin, anti-tubulin, and the goat anti-mouse or -rabbit IgG peroxidase conjugated secondary antibodies were obtained from Sigma-Aldrich (Milan, Italy).

Cell lines and treatments

Cell lines derived from HNCs of the tongue (SCC-15, CAL-27), pharynx (FaDu) or salivary gland (A-253) were from ATCC (Manassas, VA, USA) and maintained in RPMI containing 10% fetal bovine serum, 100 U/ml penicillin, and 100 µg/ml streptomycin. Neu-overexpressing salivary gland cancer cells (H-2^d) (SALTO-5) were kindly provided by Prof. F. Cavallo (University of Torino) and Prof. P. L. Lollini (University of Bologna) and kept in DMEM containing 20% fetal bovine serum (FBS). SALTO-5 cells were established from salivary carcinoma arising in BALB-*neu*T transgenic male mice hemizygous for the $p53^{172R-H}$ transgene driven by the whey acidic protein promoter[97]. Bortezomib was dissolved in DMSO. For treatments, cells were incubated for the indicated times in the presence of Bortezomib (dose range 6.25–100 nM) or vehicle control (DMSO ≤ 0.1).

Sulforhodamine B (SRB) assay

Cells were seeded at 5 x 10^3 cells/well in 96-well plates and incubated at 37° C to allow cell attachment. After 24 hours, the medium was changed and cells were incubated for 24, 48 and 72 hours with Bortezomib (6.25–100 nM) or with DMSO. Cells were then fixed with cold trichloroacetic acid (final concentration 10%) for 1 hour at 4° C. The assay was then performed as previously described[71]. The percentage survival of the cultures treated with Bortezomib was calculated by normalization of their O.D. values to those of the control cultures treated with DMSO[98]. The experiments were performed in triplicate and repeated three times.

Trypan Blue Exclusion Assay

For trypan blue exclusion assay, cells were seeded at 5 x 10^4/well in 24-well plates and incubated at 37°C to allow cells attachment. After 24 hours, the medium was changed and cells were incubated for 24, 48,

and 72 hours with Bortezomib (6.25–100 nM) or DMSO. Thereafter, adherent as well as suspended cells of each well were harvested and stained with trypan blue (Sigma-Aldrich, Milan, Italy) and counted under a light optical microscope[99]. The experiments were repeated three times, and the percentage of dead cells was compared with the total number of cells[100].

FACS analysis

Asynchronized log-phase growing cells (60% confluent, approximately 2.5 x 10^5 cells/well in 6-well plates) were treated with Bortezomib or with DMSO in a complete culture medium. Z-VAD-FMK was used at a final concentration of 40 μM for 2 hours before addition of Bortezomib. After 48 hours, adherent and suspended cells were harvested, centrifuged at 1500 rpm for 10 minutes and washed twice with cold phosphate buffered saline (PBS). The assay was then performed as previously described[101]. Cells were analyzed by flow cytometry using a FACS-Calibur cytometer running CellQuest Pro 5.2 software (BD Biosciences, San Jose, CA, USA).

Western Blotting

About 1 x 10^6 cells were seeded in 100 mm tissue culture dishes 24 hours prior to the addition of 12.5 (SCC-15 and CAL-27) or 25 nM (FaDu, A-253, SALTO-5) of Bortezomib or the vehicle control. After 24 hours (for SCC-15) and 48 hours of treatment, cells were harvested, washed twice with cold PBS and lysed in RIPA buffer as previously described[102]. For immunoblotting analysis, 15–80 μg of cell lysates (depending on the experimental setting) were resolved in 10% SDS-PAGE and then transferred to nitrocellulose membranes[103]. Equal loading and transfer of proteins was verified by Ponceau red staining of the membranes and by analyzing actin expression. The assay was then performed as previously described[72].

Native Gel Electrophoresis

Crude cell extracts (e.g., soluble fraction of the cell cytosol) were extracted under non-denaturing conditions through freeze-thawing cycles in 250 mM sucrose, 20% glycerol, 25 mM Tris-HCl, 5 mM $MgCl_2$, 1 mM EDTA, 1 mM DTT, 2 mM ATP, pH 7.4. Thereafter, lysates were cleared by centrifugation at 13000 rpm, 20 minutes, 4°C and the protein concentration was determined by Bradford assay. For each experimental condition, 75 μg of proteins were separated under native conditions employing 3.5 % acrylamide gel. Gels were then harvested in a clean dish and soaked in the reaction buffer (50 mM Tris, 5 mM $MgCl_2$, 1 mM ATP, pH 7.5), which had been supplemented with 75 μM 7-amino-4-methylcoumarin (AMC) labeled Suc - Leu - Leu - Val - Tyr -AMC peptide (referred to as LLVY-AMC) (Boston Biochem, Boston, USA), a highly specific fluorogenic substrate of the proteasome chymotrypsin-like activity. This enzymatic proteolytic activity, which has been proven to be linearly correlated with the light intensity, was then recorded through a gel-documentation system (excitation λ = 365 nm; emission λ = visible)[104]. Proteins were then transferred to a HyBond-ECL nitrocellulose filters and probed with an antibody which recognizes an epitope shared by α1–7 subunits, but not by α4 (hereafter referred to as pan-α-subunits) (Protein-tech Group, Manchester, UK), diluted 1:3000 in 0.02% Tween-PBS fat-free milk, and then

incubated with a Horseradish Peroxidase-conjugated anti-rabbit or anti-mouse IgG antibody (Biorad, Hercules, CA, USA), diluted 1:50000 in 0.2% Tween-PBS fat-free milk.

Treatment of BALB-neuT mice with Bortezomib

Transgenic BALB-*neu*T male mice were mated with BALB/c females (H-2^d; Charles River, Calco, Italy) in the animal facilities of Tor Vergata University. Founder male BALB-*neu*T mice were kindly provided by Prof. G. Forni and Prof. F. Cavallo (University of Torino, Italy)[105]. Progenies were confirmed for the presence of the transgene by PCR[106]. BALB-*neu*T mice were subcutaneously injected in the right flank with a 0.2 ml suspension containing 1 x 10^6 SALTO-5 cells in phosphate-buffered saline (PBS). Groups of BALB-*neu*T mice (8 mice per group) were treated i.p. with Bortezomib (0.5 mg/kg in 400 µl PBS + DMSO, twice a week) or with vehicle only (400 µl PBS + DMSO, twice a week) one week after the SALTO-5 tumor challenge. Mice were sacrificed at the first signs of distress[107]. The investigation has been conducted in accordance with the ethical standards and according to the Declaration of Helsinki and the ARRIVE guidelines. The work was conducted with the formal approval of the local ["Organismo Preposto al Benessere degli animali" (O.P.B.A.), University of Rome Tor Vergata] and national (Ministry of Health) animal care committees and animal experiments have been registered as legislation requires (Authorization from the Ministry of Health no. 844_2018-PR). A veterinary surgeon was present during the experiments. Animal care, before and after the experiments, was carried out only by trained personnel.

Analysis of antitumor activity in vivo

Tumor growth was monitored weekly until tumor-bearing mice were sacrificed when the tumor exceeded a 20 mm width by cervical dislocation. Tumors were measured by a caliper in two perpendicular dimensions, and the volumes were calculated using the formula: width^2 x length/2[100, 108].

Histological analysis of tumors from mice treated with Bortezomib by optical microscopy

Tumors from three animals from each group of mice were used for histological examination after hematoxylin/eosin staining using 3 µm thick paraffin sections. Necrotic areas were measured using ImageJ software on 10 microscopic fields. Immunohistochemistry (IHC) was used to analyze the presence of caspase 3-positive cells (apoptotic cells) and the expression of ErbB2, AKT and phospho-AKT in tumors from DMSO- and Bortezomib-treated mice[109]. For IHC, antigen retrieval was performed on 3 µm thick paraffin sections using EDTA citrate, pH 7.8, or citrate pH 6.0 buffers for 30 minutes at 98°C. Sections were then incubated for 1 hour at room temperature (anti-cleaved caspase 3 and anti-ErbB2 antibodies) or overnight at 4°C (anti-AKT and anti-phospho-AKT) with primary antibodies. To remove non-specific binding, slides were washed using PBS/Tween 20, pH 7.6. Antibody-antigen binding was revealed by the Horseradish Peroxidase-3,3-diaminobenzidine (HRP-DAB) Detection Kit (UCS Diagnostic, Rome, Italy). The count of cleaved caspase 3-positive cells (apoptotic cells) was performed on 10 microscopic fields at 200x magnification. Semiquantitative ErbB2, AKT and phospho-AKT expression in tumors derived from DMSO- and Bortezomib-treated mice was estimated at x200 magnification in at least 10

fields by two investigators in a blind fashion. ErbB2, AKT and phospho-AKT expression levels (negative, 0; weakly positive, 1; moderately positive, 2; strongly positive, 3) were scored. The interobserver reproducibility was > 95%. Sections were observed and photographed by Olympus BX53 light microscope[101,108,110].

Transmission electron microscopy

Ultrastructural analysis was performed on SALTO-5 cells treated with Bortezomib (12.5 nM for 24 hours) or with DMSO. After treatment, cells were fixed in 2.5% glutaraldehyde in PBS pH 7.4, and the samples were processed for ultrastructural analysis following routine procedures and observed by a Morgagni 268D transmission electron microscopy[111].

Statistical analysis

The percentage of cells survival, different phases of the cell cycle and of cells death were preliminarily verified using the Kolmogorov-Smirnov test, and the data sets were analyzed by one-way analysis of variance (ANOVA) followed by the Newman-Keuls test. Differences in the intensity of immunoreactive bands were evaluated by a two-tailed Student's t-test or one-way ANOVA followed by Tukey's post-hoc significance test. Values with $p \leq 0.05$ were considered significant. Survival curves and tumor volumes were analyzed using the Kaplan-Meier method and compared with a log-rank test (Mantel-Cox). Differences in tumor volumes were regarded as significant when the *p-value* was ≤ 0.05.

Results

Inhibition of pharynx (FaDu), tongue (SCC-15, CAL-27) and salivary gland (A-253, SALTO-5) cancer cells survival by Bortezomib

The survival of pharynx (FaDu), tongue (SCC-15, CAL-27) and salivary gland (A-253) cancer cells was evaluated by the SRB assay after exposure to increasing doses of Bortezomib (6.25-12.5-25-50-100 nM) or vehicle control (DMSO) for 24, 48 and 72 hours. The effect of Bortezomib was also analyzed in SALTO-5 cells in order to establish whether this mouse cell line was susceptible to the *in vitro* anti-tumoral activity of Bortezomib and thus it could be used as transplantable tumor cell line in BALB-*neu*T mice to determine the *in vivo* anti-tumoral effect of the drug.

The effect of Bortezomib on cells proliferation was dose- and time-dependent as compared to control cells. The greatest effect was obtained at the concentrations of 25, 50 and 100 nM and after 48 and 72 hours of treatment (Fig. 1). SCC-15 were the most sensitive cells to the drug's effect.

In addition, the concentration of Bortezomib that inhibited 50% of cells growth (IC_{50}) after 48 and 72 hours was also determined. FaDu cells were the most resistant to Bortezomib activity, while SCC-15 was the most sensitive cell line (Table 1).

Table 1
Half maximal inhibitory concentration (IC_{50}) of Bortezomib in inhibiting cell growth of SCC-15, CAL-27, FaDu, A-253 and SALTO-5 cell lines after 48 and 72 hours of treatment.

Cell line	Treatment (hours)	IC_{50} ± SD (nM)
SCC-15	48	19.89 ± 3.46
	72	11.04 ± 0.26
CAL-27	48	33.73 ± 1.91
	72	15.97 ± 3.61
FaDu	48	67.83 ± 5.45
	72	32.92 ± 2.26
A-253	48	55.90 ± 19.01
	72	10.25 ± 1.50
SALTO-5	48	60.65 ± 7.83
	72	10.79 ± 1.84

Effects of Bortezomib on cell death of pharynx (FaDu), tongue (SCC-15, CAL-27) and salivary gland (A-253, SALTO-5) cancer cell lines

The death of human (FaDu, SCC-15, CAL-27, A-253) and mouse (SALTO-5) HNC cells was evaluated by the Trypan blue exclusion assay after exposure to increasing doses of Bortezomib (6.25–100 nM) or vehicle control (DMSO) for 24, 48 and 72 hours. The dye exclusion assay was used to determine the number of viable HNC cells upon Bortezomib exposure. Bortezomib significantly increased the percentage of cell death in a dose- and time-dependent manner in all cell lines as compared to vehicle control after 24, 48 and 72 hours (Fig. 2).

Effects of Bortezomib on apoptosis and cell cycle distribution of HNC cell lines

To evaluate the effects of Bortezomib on apoptosis and cell cycle distribution, FACS analysis of DNA content was performed on HNC cells treated with increasing doses of Bortezomib (6.25-50 nM) for 48 hours; DMSO was used as control vehicle. Our results showed that treatment with Bortezomib significantly increased the percentage of cells in the subG1 phase at all doses in SCC-15, CAL-27 and A-253 cells, at 25–50 nM in the FaDu cells and at 12.5-25-50 nM in SALTO-5 cells. An increasing content of the hypodiploid DNA in the subG1 phase is typical of apoptosis. The treatment with Bortezomib also

induced, at all doses tested, a significant increase in A-253 cells for the percentage of cells in the G2/M phase (Table 2).

To confirm the induction of apoptosis, cells were simultaneously treated with Bortezomib at the highest dose and with the universal caspase inhibitor, Z-VAD-FMK. Administration of this drug was able to significantly reduce the number of cells in the subG1 phase as compared to the single treatment with Bortezomib at the highest dose, thus suggesting the induction of cell death by apoptosis following treatment with Bortezomib in HNC cell lines (Table 2).

Table 2

Effect of Bortezomib on the cell cycle of cell lines of carcinomas of the pharynx (FaDu), of the tongue (SCC-15, CAL-27) and of the salivary gland (A-253, SALTO-5) following 48 hours of treatment.

	nM	subG1[a]	*p**	G0/G1	*p*	S	*p*	G2/M	*p*
SCC-15	DMSO	3.00 ± 0.06		64.04 ± 0.25		6.60 ± 0.21		26.71 ± 0.16	
	Bor 6.25	28.40 ± 0.69	< 0.01	50.01 ± 0.53	< 0.001	6.84 ± 0.10		15.11 ± 0.08	< 0.001
	Bor 12.5	72.19 ± 0.19	< 0.001	25.29 ± 0.44	< 0.001	2.03 ± 0.16	< 0.001	0.89 ± 0.16	< 0.001
	Bor 25	85.62 ± 0.91	< 0.001	13.91 ± 0.86	< 0.001	0.48 ± 0.12	< 0.001	0.21 ± 0.07	< 0.001
	Bor 50	91.47 ± 0.66	< 0.001	8.25 ± 0.58	< 0.001	0.21 ± 0.06	< 0.001	0.26 ± 0.13	< 0.001
	Bor50 + Z-VAD	60.28 ± 0.79	< 0.001	27.55 ± 0.46	< 0.001	5.56 ± 0.11	< 0.001	7.02 ± 0.12	< 0.001
CAL-27	DMSO	3.03 ± 1.17		66.04 ± 0.25		10.24 ± 0.22		20.96 ± 1.17	
	Bor 6.25	38.72 ± 0.39	< 0.001	39.75 ± 0.17	< 0.001	10.53 ± 0.22		11.45 ± 0.32	< 0.001
	Bor 12.5	76.92 ± 0.11	< 0.001	18.15 ± 0.39	< 0.001	3.07 ± 0.42	< 0.001	2.21 ± 0.08	< 0.001
	Bor 25	86.52 ± 1.15	< 0.001	11.04 ± 0.79	< 0.001	1.47 ± 0.15	< 0.001	1.19 ± 0.35	< 0.001
	Bor 50	84.36 ± 1.05	< 0.001	11.77 ± 0.69	< 0.001	1.68 ± 0.08	< 0.001	2.39 ± 0.32	< 0.001
	Bor50 + Z-VAD	42.22 ± 0.57	< 0.001	23.16 ± 0.66	< 0.01	14.17 ± 0.23	< 0.001	20.89 ± 0.45	< 0.001
FaDu	DMSO	1.13 ± 0.06		56.01 ± 1.11		9.50 ± 1.77		33.81 ± 0.71	
	Bor 6.25	1.44 ± 0.69		54.39 ± 0.84		8.92 ± 0.34		35.73 ± 1.24	
	Bor 12.5	1.84 ± 0.05		53.19 ± 1.41		11.11 ± 0.86		34.38 ± 2.26	

[a]The percentage of cells in phase subG1, G0/G1, S and G2/M was calculated using the CellQuest Pro 5.2 software. Results represent the mean ± SD (standard deviation) of two experiments. *The statistical significance of the effect obtained with the treatment with Bortezomib (Bor) was calculated with respect to that obtained with the vehicle alone (DMSO). The statistical significance of the effect obtained with Bortezomib at a dose of 50 nM was also calculated with respect to that obtained in cells treated with Bortezomib at a dose of 50 nM together with the Z-VAD-FMK inhibitor (Bor50 + Z-VAD). NS: not significant.

	nM	subG1[a]	*p**	G0/G1	*p*	S	*p*	G2/M	*p*
	Bor 25	10.82 ± 0.21	< 0.001	47.50 ± 0.42	< 0.01	11.21 ± 0.16		31.00 ± 0.61	
	Bor 50	18.65 ± 0.40	< 0.001	44.46 ± 0.72	< 0.001	9.24 ± 0.26		28.22 ± 0.54	< 0.05
	Bor50 + Z-VAD	3.58 ± 0.23	< 0.001	39.24 ± 0.46	< 0.05	12.06 ± 0.29	< 0.01	45.65 ± 0.34	< 0.001
A-253	DMSO	2.15 ± 0.20		56.74 ± 0.28		5.58 ± 0.25		35.78 ± 0.62	
	Bor 6.25	8.50 ± 0.21	< 0.001	26.36 ± 0.42	< 0.001	6.59 ± 0.29	< 0.05	59.10 ± 1.23	< 0.001
	Bor 12.5	9.93 ± 0.11	< 0.001	19.51 ± 0.04	< 0.001	9.84 ± 0.66	< 0.001	61.32 ± 0.47	< 0.001
	Bor 25	9.63 ± 0.39	< 0.001	26.78 ± 0.82	< 0.001	15.64 ± 0.08	< 0.001	48.72 ± 1.12	< 0.001
	Bor 50	9.66 ± 0.04	< 0.001	33.12 ± 0.80	< 0.001	16.56 ± 0.52	< 0.001	41.55 ± 0.31	< 0.001
	Bor50 + Z-VAD	5.14 ± 0.33	< 0.001	23.24 ± 0.06	< 0.001	12.01 ± 0.15	< 0.001	60.33 ± 0.30	< 0.001
SALTO-5	DMSO	1.40 ± 0.12		24.58 ± 0.25		5.11 ± 0.30		69.20 ± 0.40	
	Bor 6.25	1.00 ± 0.15		22.99 ± 1.75		4.48 ± 0.56		71.77 ± 2.34	
	Bor 12.5	6.74 ± 0.30	< 0.001	20.17 ± 0.73	< 0.01	4.59 ± 0.28		68.74 ± 0.82	
	Bor 25	23.23 ± 0.11	< 0.001	17.93 ± 0.34	< 0.01	4.34 ± 0.31		54.75 ± 0.66	< 0.001
	Bor 50	30.31 ± 0.09	< 0.001	18.72 ± 0.17	< 0.01	4.49 ± 0.25		46.90 ± 0.06	< 0.001
	Bor50 + Z-VAD	19.29 ± 0.49	< 0.01	18.78 ± 0.14		5.80 ± 0.04	< 0.05	56.48 ± 0.37	< 0.001

[a]The percentage of cells in phase subG1, G0/G1, S and G2/M was calculated using the CellQuest Pro 5.2 software. Results represent the mean ± SD (standard deviation) of two experiments. *The statistical significance of the effect obtained with the treatment with Bortezomib (Bor) was calculated with respect to that obtained with the vehicle alone (DMSO). The statistical significance of the effect obtained with Bortezomib at a dose of 50 nM was also calculated with respect to that obtained in cells treated with Bortezomib at a dose of 50 nM together with the Z-VAD-FMK inhibitor (Bor50 + Z-VAD). NS: not significant.

Effect of Bortezomib on the expression of molecules involved in apoptosis in HNC cell lines

To corroborate that Bortezomib treatment induced apoptosis, the expression of Bax, Bcl-2, procaspases 9/8/3, caspase 9/8/3 and cleavage of poly (ADP-ribose)polymerase-1 (PARP-1) was analyzed by Western blotting after treatment of cells with different concentrations of Bortezomib, as indicated in Fig. 3. Our results showed that Bortezomib treatment significantly increased the Bax/Bcl-2 ratio in CAL-27 (p = 0.023), A-253 (p = 0.0007) and SALTO-5 (p = 0.0015) cells. In SCC-15 and FaDu cells this ratio remained unchanged as compared to control cells. However, the activation of the intrinsic pathway of apoptosis was observed in all cell lines. Indeed, our results showed that Bortezomib treatment was able to induce the release of the active fragment of procaspase-9 in SCC-15, FaDu and SALTO-5 cells and to reduce the expression of procaspase 9 in the other cell lines, thus suggesting the activation of the molecule (CAL-27, p = 0.0033; A-253, p = 0.0025). In addition, the activation of the extrinsic pathway of apoptosis was observed as well in SCC-15, CAL-27 and A-253 cells, as indicated by the cleavage of the procaspase 8 in the activated fragments p43/41. In the other cell lines, the activation of the extrinsic pathway of programmed cell death was not detected (Fig. 3).

Activated caspase 9/8 can cleave and activate caspase 3, inducing the proteolytic inactivation of PARP-1, which is involved in DNA repair and genomic integrity. Indeed, our results showed that Bortezomib caused in all cell lines the proteolytic cleavage of caspase 3 into the activated fragments p19 and p17, and the proteolytic cleavage of PARP-1 in SCC-15, CAL-27 and A-253 cells (Fig. 3).

Effects of Bortezomib on the expression and activation of ErbB receptors (EGFR and ErbB2) and pro-survival signaling transduction pathway molecules (ERK, JNK, p38, AKT) in HNC cell lines

The MAP (Mitogen Activated Protein) kinase transduction pathway is triggered by the activation of EGFR and ErbB2/*neu* tyrosine kinase receptors. It has been demonstrated that HNC cell lines overexpress EGFR and ErbB2 receptors, which play a role in their cellular transformation[35].

Our results indicated that Bortezomib significantly decreased the level of EGFR and ErbB2 expression in SCC-15 (p = 0.0014, for EGFR; p = 0.0006, for ErbB2), CAL-27 (p = 0.013, for EGFR; p = 0.0018, for ErbB2), A-253 (p = 0.0067, for EGFR; p = 0.002, for ErbB2) cells as compared to control cells. Only a decreased expression of ErbB2/*neu* (p = 0.007) was observed in the murine cell line SALTO-5. In contrast, the expression of these receptors remained unchanged in FaDu cell line (Fig. 4).

In addition, we evaluated the effect of Bortezomib on the expression and phosphorylation of MAP kinases ERK, JNK and p38. Our results showed that Bortezomib inhibited the phosphorylation of ERK1 and ERK2 in SCC-15 (p = 0.0027, for pERK1; p = 0.0009, for p-ERK2) and A-253 (p = 0.0043, for pERK1; p = 0.0003, for pERK2) cells as compared to untreated cells. In addition, Bortezomib treatment decreased the level of phosphorylation of ERK2 in FaDu cells (p = 0.016), while it increased it in SALTO-5 cells (p = 0.019). Bortezomib did not affect the levels of phosphorylation of ERK1/2 in CAL-27 cells (Fig. 4).

Furthermore, it was observed that Bortezomib decreased the level of phosphorylation of JNK p54 in SCC-15 cells ($p = 0.006$), while increased it in CAL-27 ($p = 0.0016$) and that of JNK p46 in SCC-15 ($p = 0.022$), A-253 ($p = 0.020$) and SALTO-5 cells ($p = 0.009$). Bortezomib decreased the p38 phosphorylation in CAL-27 ($p = 0.0037$), and SALTO-5 ($p = 0.002$) cells, while the p38 phosphorylation was enhanced in SCC-15 cells ($p = 0.003$). Bortezomib did not affect the phosphorylation of p38 in FaDu and A-253 cells (Fig. 4).

Finally, we evaluated whether Bortezomib treatment inhibited the expression and phosphorylation of the pro-survival kinase AKT, which promotes tumor growth[36]. Our results indicated that Bortezomib decreased AKT phosphorylation in SCC-15 ($p < 0.001$), CAL-27 ($p = 0.0011$), A-253 ($p < 0.001$) and SALTO-5 cells ($p < 0.001$) (Fig. 4).

Effects of Bortezomib on autophagy of HNC cell lines

To determine the effect of Bortezomib in the induction of autophagy, HNC cell lines were analyzed for the expression of Beclin-1, LC3-I, LC3-II and p62 upon treatment by western blotting. Our results showed that Bortezomib significantly increased Beclin-1 expression in SCC-15 ($p = 0.0007$) and A-253 ($p = 0.0015$) cells, while it was decreased in CAL-27 ($p = 0.0005$), FaDu ($p = 0.011$) and SALTO-5 ($p = 0.0021$) cells (Fig. 5). The activation of the autophagic process can be revealed by the conversion of the cytosolic form LC3-I into the membrane-bound form LC3-II, which is localized in the autophagosomes[37,38]. Our results showed that LC3-I and LC3-II were constitutively expressed in DMSO-treated cells. Bortezomib significantly increased the expression of LC3-I (SCC-15, $p = 0.0011$; CAL-27, $p = 0.0011$; FaDu, $p = 0.0012$; A-253, $p = 0.0008$) and LC3-II (SCC-15, $p = 0.006$; CAL-27, $p = 0.031$; FaDu, $p = 0.021$; A-253, $p = 0.039$) in all human cell lines. An increase of only LC3-I expression was observed in SALTO-5 cells ($p = 0.0018$) (Fig. 5). In addition, Bortezomib induced the increase of p62 in SCC-15 ($p = 0.0007$), CAL-27 ($p = 0.00015$), FaDu ($p = 0.00014$), A-253 ($p = 0.0008$) cell lines, while its expression did not change in SALTO-5 cells (Fig. 5). These results suggest that Bortezomib induced accumulation of p62 and LC3-II, which is indicative of a blocked autophagy[39].

Validation of proteasome inhibition by Bortezomib in HNC cell lines

In order to evaluate the effectiveness of proteasome inhibition in HNC cells by Bortezomib and to determine whether resistance to the drug may have occurred, FaDu, SCC-15, CAL-27, A-253 and SALTO-5 cells were treated with the Bortezomib by following a scheme and doses based on results from the IC_{50} values (see Fig. 2). At the indicated time points, Bortezomib- and DMSO-treated cells were harvested and the cytosolic fraction (i.e., where proteasome is mainly represented) was isolated through a non-denaturing lysis procedure. For every cell line, proteasome inhibition and individual particles content was first assayed by native gel electrophoresis[40] (see Materials and Methods for further details) (Fig. 6).

For all cell lines, a marked inhibition of the activity of all three main assemblies existing in the cell cytosol (*i.e.*, the uncapped 20S, the doubly 19S:20S:19S and single-capped 19S:20S, respectively) was observed

in the presence of Bortezomib (Fig. 6a). With respect to control cells, SCC-15, CAL-27 and SALTO-5 cells displayed the greatest extent of proteasome inhibition (> 50%) in the presence of the lowest Bortezomib concentration (25 nM in SCC-15 and SALTO-5, 12 nM in CAL-27) at the first time-point (7 hours in SCC-15 and 12 hours in SALTO-5 and CAL-27) of stimulation (Fig. 6a, *upper panel*; Supplementary Fig. S1). Conversely, in the case of A-253 cells, a > 50% extent of proteasome inhibition at 12 hours of stimulation was achieved only at 50 nM Bortezomib. Interestingly, FaDu cells showed a less marked inhibition of proteasome activity as compared to the other cell lines. The extent of inhibition was roughly 50% in the presence of either 25 nM or 50 nM Bortezomib at 12 hours and slightly lower at 24 hours (Fig. 6a, *upper panel*; Supplementary Fig. S1). A modest rescue of proteasome activity was further observed in SALTO-5 cells stimulated with 25 nM and 50 nM Bortezomib for 24 hours, as compared to the effect induced by the same Bortezomib concentrations after 12 hours of stimulation (Fig. 6a, *upper panel*; Supplementary Fig. S1). In the case of SCC-15 cells, an unexpected finding was observed. The overall proteolytic activity was found to decrease in untreated cells over time (14 hours *vs* 7 hours) (Fig. 6a *upper panel*; Supplementary Fig. S1).

In accordance with a general inhibition of proteasome activity, the poly-ubiquitinated proteins, (*i.e.*, the natural substrates of capped proteasome assemblies), which were assayed by denaturing and reducing Western blotting, turned out to be significantly increased in the presence of Bortezomib under all experimental conditions (Supplementary Fig. S2).

To further validate their identity, proteasome particles were then transferred to a nitrocellulose filter and probed with an antibody which recognizes all catalytic assemblies of proteasome (*i.e.*, 30S, 26S, and 20S), since it is raised against a peptide covering residues shared by the α1–7 subunits of 20S proteasome, with the exception of α4 (hereafter referred to as pan-α-subunits). By probing the filters some unexpected findings were observed (Fig. 6a, *bottom panel*, and Fig. 6b). First of all, proteasome particles immuno-staining was significantly impaired over the whole time-interval (*i*) in FaDu cells under all tested conditions, (*ii*) in SCC-15 cells stimulated with 25 and 50 nM Bortezomib for 7 hours and (*iii*) in A-253 and CAL-27 cells stimulated with the highest Bortezomib concentrations (*i.e.*, 50 nM and 25 nM, respectively) (Fig. 6a, *bottom panel*, and Fig. 6b); (iv) in SALTO-5 cells treated with 50 nM Bortezomib over 12 hours. Remarkably, regardless the dose and time of Bortezomib incubation, FaDu cells treated with Bortezomib showed the appearance of non-canonical proteasome assemblies with an apparent mass/charge ratio very similar to that reported by other authors in a similar experimental condition[41] (Fig. 6a, *bottom panel*, red arrow). It is worth pointing out that SCC-15 cells displayed a decrease in overall proteasome content also in control cells harvested after 14 hours (with respect to control cells harvested after 7 hours), thus confirming the observed loss of proteasome activity (Fig. 6). Conversely, SALTO-5 cells appeared to be somewhat resistant to this phenomenon, since this cell line did not display any significant decrease of proteasome particles content (Fig. 6a, *bottom panel*, and Fig. 6b) with the exception of cells treated with 50 nM for 12 hours.

In addition, A-253 and CAL-27 cells displayed a very high 20S/capped assemblies (30S + 26S) ratio, even though the pattern of activity (Fig. 6a, *bottom panel*, and Fig. 6b) was comparable to that of other cell

lines analyzed which showed a more balanced 20S/capped assemblies ratio.

To better address these findings, the same crude cell extracts, run by native gel electrophoresis, were analyzed by denaturing, and reducing Western blotting. Interestingly, the content of free α7 and Rpt5 subunits, which are representative of the 20S and 19S particles, respectively, ranged from unchanged or even increased under the investigated experimental conditions (Supplementary Fig. S2).

To further verify the observed phenomenon, FaDu cells, which displayed the apparent highest extent of proteasome loss, were further stimulated with 25 and 50 nM Bortezomib for 30 minutes and 2 hours (Fig. 7). Proteasome activity was almost null as early as after 30 minutes of stimulation in the presence of 50 nM Bortezomib, whilst a residual activity was observed in the presence of 25 nM Bortezomib (Fig. 7, *left panel*). After 2 hours of stimulation, the proteolytic activity was undetectable in the presence of all Bortezomib concentrations. Interestingly, by probing the filter with the anti-pan-α subunits antibody, it was observed that the proteasome assemblies were unaffected by Bortezomib after 30 minutes of stimulation (Fig. 7, *left panel*). Conversely, after 2 hours of Bortezomib treatment, a very robust loss of proteasome assemblies was observed in the presence of 50 nM Bortezomib, whereas residual proteasome assemblies were detected in the presence of 25 nM Bortezomib (Fig. 7, *right panel*).

Bortezomib inhibited the in vivo growth of SALTO-5 cells transplanted in BALB-neuT mice

Treatment with Bortezomib significantly affected tumor growth *in vivo*. BALB-*neu*T mice were subcutaneously injected in the right flank with SALTO-5 cells and treated i.p. with Bortezomib. Tumor volumes in the Bortezomib-treated mice were significantly less than those in the control-treated mice after 3 weeks (53.1 *vs* 90.5 mm^3; $p = 0.030$). This significant difference was maintained until the 5th week, when two control-treated mice were sacrificed due to the excessive size of the tumor (251.6 *vs* 1035 mm^3; $p = 0.0001$). The remaining control-treated mice were sacrificed at 6 (5 mice) and 7 (1 mouse) weeks (Fig. 8a). At this stage (7 weeks after tumor challenge) only one Bortezomib-treated mouse was sacrificed due to excessive size of the tumor. In contrast, the remaining Bortezomib-treated mice were sacrificed at week 9 (3 mice), 10 (2 mice), 11 (1 mouse) and 12 (1 mouse). The mean survival significantly increased for the mice treated with Bortezomib, as compared to the control-treated mice (9.5 *vs* 6 weeks, Bortezomib-treated mice *vs* control-treated mice; $p = 0.0001$) (Fig. 8b), indicating that the risk of SALTO-5 cell growth in control-treated mice was 22.57 times greater than that of mice treated with Bortezomib (Table 3). Our results demonstrated that treatment with Bortezomib interfered with the *in vivo* tumor growth of transplanted salivary gland cancer cells SALTO-5.

Table 3
Analysis of the survival of BALB-*neu*T mice after treatment with Bortezomib by the log-rank test (Mantel-Cox).

Variable	Contrast	Hazard Ratio	95% Hazard Ratio Confidence Limits		*p* Value	Median Survival (Weeks)
			Lower	Upper		
Treatment	Ctr *vs* Bortezomib	22.57	4.524	112.6	0.0001	6 *vs* 9.5

Histological analysis of tumors from mice treated with Bortezomib by Optical Microscopy

Histological examination of tumors from control mice (PBS + DMSO) showed the presence of solid tumors with the histological features of the adenocarcinomas; very small areas of cellular alterations and/or necrosis were observed. In contrast, histological examination of tumors from Bortezomib-treated mice (Bor) showed extensive necrosis as compared to control mice (41.5 ± 14.5 *vs* 1.8 ± 0.2 percentage of necrotic areas/microscopic field, $p = 0.0015$) (Fig. 9).

The presence of apoptotic cells was evaluated by the expression of cleaved caspase 3 in cancer cells employing immunohistochemical analysis (Fig. 9). The number of apoptotic cells within the tumors from Bortezomib-treated mice (62.8 ± 5.1) was higher than that from control-treated mice (8.4 ± 1.1) ($p = 0.0001$).

The expression of ErbB2 on tumor cells *in vivo* was evaluated by immunohistochemical analysis as well (Fig. 9). Tumors from Bortezomib-treated mice showed a significantly lower expression of ErbB2 than that from control-treated mice (1.0 ± 0.4 *vs* 2.3 ± 0.8 staining intensity, $p = 0.04$). In addition, AKT phosphorylation was significantly decreased in tumors from mice treated with Bortezomib, as compared to those treated with DMSO (0.3 ± 0.2 *vs* 0.8 ± 0.2 staining intensity, $p = 0.04$). On the other hand, the same treatment did not affect AKT expression in tumors (Fig. 9).

Ultrastructural analysis of SALTO-5 cells in vitro treated with Bortezomib

Ultrastructural analysis was performed by transmission electron microscopy on SALTO-5 cells treated with Bortezomib or DMSO at the concentration of 25 nM for 24 hours. DMSO-treated cells showed heterogeneous forms with a predominance of round over stretched cells. The nuclei appeared large, mainly formed by euchromatin with low dense heterochromatin in the periphery. In the cytoplasm several mitochondria and cisterns of rough endoplasmic reticulum were detected, with few vacuoles (Fig. 10a,b). Conversely, Bortezomib-treated cells showed mainly necrotic features (Fig. 10c) with cytoplasm swelling and the presence of numerous cytoplasmic vacuoles surrounded by a single or double membrane, the latter being probably of autophagic origin (Fig. 10d). Few apoptotic cells were also visible (Fig. 10e).

Discussion

The use of new therapeutic agents is being evaluated in HNC[5–8]. Among these, inhibitors of the UPS, and mainly of proteasome, are assuming particular importance. The proteasome is a multisubunit complex, which is responsible for the selective proteolysis of damaged, denatured or structurally aberrant proteins[42]. The purpose of proteasome inhibitors is to block the degradation of the altered proteins, performed by this complex, stimulating their building up in intracellular compartments, thus bringing about the formation of a toxic environment and the subsequent need to activate apoptotic processes[43]. Bortezomib ([(1*R*)-3-methyl-1-({(2*S*)-3-phenyl-2-[(pyrazin-2-ylcarbonyl)amino]propanoyl}amino)butyl]boronic acid) is a boronic acid derivative which contains pyrazinoic acid, phenylalanine and leucine with boronic acid within its structure. It is a specific and reversible inhibitor of the chymotrypsin-like activity of the 20S proteasome[14,20,21]. Bortezomib has been reported to possess potent anticancer activity, both *in vitro* and *in vivo*, in prostate cancer, pancreatic cancer, renal cell carcinoma, and squamous cell carcinoma[23–26,44,45].

Preclinical studies have shown that Bortezomib, when used alone, inhibited cells growth, induced apoptosis, autophagy, and modulation of individual signaling transduction pathways in HNSCC (Head and neck squamous cell carcinoma) cells *in vitro*[46–56]. However, none of these studies have analyzed the simultaneous effects of Bortezomib on proteasome, apoptosis, autophagy and signaling transduction pathways involved in cellular transformation in HNC cell lines. Thus, one of the novelties of our study is the detailed analysis of the correlation between inhibition of the proteasome and activation of apoptosis, autophagy and modulation of cell survival signaling transduction pathways, that is a concern which no previous single study has been dealing with. Bortezomib was previously shown to activate apoptosis by modulating the expression of pro-apoptotic and anti-apoptotic proteins[48,49] following the activation of caspases and/or the cleavage of PARP-1 protein[46,48,50–52,57] and hypodiploidia and phosphatidylserine externalization in HNSCC cell lines[46,48,56]. Bortezomib was shown to stimulate autophagy in HNSCC cells in two studies showing autophagosomes formation, upregulation of LC3-I, -II, Beclin-1 and the JNK-dependent phosphorylation of Bcl-2 after bortezomib treatment[58,59]. It was also suggested that autophagy attenuated the Bortezomib cytotoxicity[59]. Bortezomib was able to modulate expression and activation of signaling pathways in HNSCC. Two studies demonstrated Bortezomib inhibition of AKT activation and mTOR in HNSCC cell lines[46,60]. Other studies demonstrated the upregulation of STAT3 after Bortezomib treatment and the anti-tumoral efficacy of a co-treatment with STAT3 inhibitors in HNSCC cells[55]. Only two studies showed that Bortezomib affects proteasome activity by inducing the accumulation of ubiquitylated proteins in larynx (UM-SCC-11A, -11-B) [56] and mouth floor (SCC1) cell lines[59]. It is worth pointing out that the majority of these studies investigated the effect of Bortezomib in the modulation of individual biological pathways being restricted to SCC cell lines arising in head and neck. In our study the *in vitro* and *in vivo* effects of Bortezomib were for the first time analyzed in a salivary gland adenocarcinoma experimental model. Salivary gland carcinomas represent 6–8% of HNC, with heterogeneous morphologies and clinical outcomes[3]. The mainstream therapy for these types of

cancer, when feasible, is the surgery followed by radiation therapy. The chemotherapy has demonstrated mixed results with low responses for advanced or metastatic malignant tumors, so that new targeted therapies are under evaluation[61–63]. Bortezomib has been evaluated for the treatment of only adenoid cystic carcinoma in combination with doxorubicin in a phase II trial, leading to no complete or partial responses in patients[32].

We demonstrated that Bortezomib inhibited in a dose- and time-dependent manner the growth and induced cell death of SCC cells from tongue (SCC-15 and CAL-27), pharynx (FADU) and of salivary gland adenocarcinoma (A-253). The tongue cell line SCC-15 turned out to be the most sensitive one to the effect of the drug, whereas the pharyngeal carcinoma cell line (FaDu) was the most resistant to the action of Bortezomib.

We demonstrated that treatment with Bortezomib significantly increased the percentage of cells in the subG1 phase, which is conventionally associated with apoptotic phenomena. The use of the inhibitor Z-VAD-FMK further confirms the induction of cell death by apoptosis following treatment with Bortezomib in these cell lines. In addition, Bortezomib induced a significant increase in the percentage of cells in the G2/M phase at all doses in the A-253 cell line, thus suggesting the induction of apoptosis and a cell cycle block in the G2/M phase. It is worth remarking that only the salivary gland adenocarcinoma A-253 cell line showed a G2/M arrest simultaneous to apoptosis, thus indicating a different response to the drug. This cell cycle pattern after Bortezomib treatment was previously reported in tumor cell lines from larynx cancer[56], colorectal cancer[64], non-small cell lung carcinoma[65], prostate cancer[43], Ewing's sarcoma[66], malignant mesothelioma and breast cancer[67].

Our findings of apoptosis activation by Bortezomib corroborated previous results employing HNSCC cell lines[46–52] and showed for the first time Bortezomib-mediated apoptosis in a salivary gland adenocarcinoma cell line (A-253).

The pathway of MAP kinases family (Mitogen Activated Protein kinases) is one of the main signal transduction pathways triggered by EGFR and ErbB2. It has been shown that these receptors are often over-expressed and play a role in the carcinogenesis process of HNC[35]. Our results indicated that Bortezomib significantly decreased the expression level of EGFR and/or ErbB2 in SCC-15, CAL-27, and A-253 cells but not in FaDu cells. Accordingly, the decreased expression of the ErbB2 receptor only in tongue, salivary gland but not pharynx cell lines is an additional finding which outlines Bortezomib-mediated biological effect in a cell line specific-dependent modality. One study showed that Bortezomib was not able to modulate EGFR expression in HNSCC cell lines[57]. EGFR and ErbB2 are frequently over-expressed in HNC cells[35,68] and are frequently prone to heterodimerization that confers tumor growth advantage[69,70].

To better elucidate the possible intracellular signaling mechanisms involved in the effects of Bortezomib, we have analyzed the phosphorylation status of ERK1/2, p38 and JNK/SAPK kinases (p46/p54), important members of the serine/threonine MAP kinase family. As a matter of fact, the activation of

ERK1/2 can promote proliferation, differentiation, adhesion, migration, and survival but also apoptosis[71–74]. In addition, the activation of p38 and JNK1/2 stress pathways modulates cell proliferation, differentiation, and apoptosis[75,76] and Bortezomib-induced activation of p38 and JNK is associated with the induction of apoptosis in several types of cancer[77,78]. Our findings showed that the treatment with Bortezomib was able to inhibit the phosphorylation of ERK1 and/or ERK2 in FaDu, SCC-15 and A-253 cells. Our results showed that the effect of Bortezomib on the modulation of the p38 activation was cell lines dependent. Bortezomib induced an increase in the phosphorylated form of JNK p54 and/or p46 in CAL-27, SCC-15, and A-253 cells but not in FaDu cells. This finding corroborated other studies in which it has been shown that Bortezomib induced apoptosis by activating JNK kinase[79] in multiple myeloma[80, 81] and in non-small cell lung cancer[82]. Our finding extends this observation to the salivary gland adenocarcinomas cell line. In addition, other studies have shown that the activation of JNK kinase is necessary for the activation of death by autophagy in HNSCC cell lines[47,58]. Accordingly, our results showed that Bortezomib induced autophagy in human HNSCC cells, but the process was then blocked, as showed by the increase of p62[39]. The same effect was observed for the first time in the salivary gland adenocarcinoma cell line. The block of the autophagic flux by Bortezomib was reported in ovarian cancer cells, hepatocellular carcinoma cells and endometrial cancer cells[83], breast cancer cells[84], and B-Raf-mutated melanoma cells[85].

Furthermore, we evaluated the *in vitro* effect of Bortezomib on the activation of the serine/threonine kinase AKT, which plays a role in various physiological processes, such as differentiation and cell cycle, transcription and translation, metabolism, and apoptosis. AKT activation, which occurs through phosphorylation of serine 273, depends on the activation of phosphatidyl inositol 3 kinase (PI3K) and triggers a cell survival signal[86]. Our results showed that treatment with Bortezomib results in the inhibition of AKT phosphorylation in both the tongue squamous carcinoma cell lines (SCC-15, CAL-27) and in the salivary gland adenocarcinoma cell line (A-253 cells) which was accompanied by a significant decrease in the expression of the total form of AKT in these cell lines. The inhibition of AKT phosphorylation by Bortezomib is a key molecular event for Bortezomib-mediated apoptosis in HNC[46, 60] and non-small cell lung cancer cells[82]. However, our findings showed that Bortezomib had no effect on AKT expression and phosphorylation on the pharynx cell line FaDu.

Finally, the efficacy of proteasome inhibition by Bortezomib *in vitro* was investigated focusing on whether different responses on the modulation of the signaling pathway molecules were dependent on a different sensibility of cells to Bortezomib-induced inhibition of proteasome activity. Only two studies showed that Bortezomib affects proteasome activity by inducing the accumulation of ubiquitylated proteins in larynx[56] and mouth floor cells[59]. Thus, a further novelty of our study is the analysis of the structural and functional effects of Bortezomib on the proteasome assemblies in HNC cell lines. On the other hand, our results uncover some findings which are worth being further discussed. Although every cell line displayed sensitivity to Bortezomib treatment, some differences were observed. Thus, the different responses observed upon Bortezomib treatment in the HNC cell lines could be due to a different extent of

proteasome inhibition. Indeed, FaDu cells, which were reported to be the most resistant to Bortezomib treatment in terms of viability, were those displaying the lowest extent of proteasome inhibition after 12 hours and 24 hours of stimulation, regardless the Bortezomib concentration administered. It is important to know that, as highlighted above, Bortezomib was not able to induce modulation of EGFR, ErbB2, JNK, p38 as well AKT proteins in FaDu cells. The ineffectiveness of Bortezomib in modulating these signal transduction pathways thus parallels the low efficacy of Bortezomib in inhibiting the proteasome activity.

However, the Bortezomib inhibitory effect on overall proteolytic activity was several-fold greater when the proteasome assemblies were harvested and analysed at earlier time-points. Without ruling out the possibility that FaDu cells may have evolved canonical mechanisms of drug resistance (*e.g.*, drug secretion and/or detoxification, or selective downregulation of 19S subunits[87]), the resistance of these cells to Bortezomib-induced apoptosis, which is in sharp contrast with the complete early proteasome inhibition after 2 hours, can be likely explained through two different and not mutually exclusive hypotheses, namely: *i)* Bortezomib, being a reversible inhibitor, is displaced from the β5 catalytic site at a higher rate than in other cells; *ii)* among all cells employed in this study, FaDu are those which more readily synthesize *de novo* proteasome assemblies. Hypothesis *i)* indeed reflects a chemical property of Bortezomib which contributes to the resistance through which the cells can bypass the drug-induced death. However, although speculative at this stage, we envisage that hypothesis *ii)* may be of greater relevance to explain the observed behaviour for two main reasons:

- FaDu cells were the only cells clearly inducing the formation of alternative proteasome assemblies, displaying an electrophoretic pattern (mass/charge) of the species after 12 hours and 24 hours (but not at 20 minutes or 2 hours), which clearly resembles that of non-canonical complexes, such as PA28-20S; thus, the formation of these alternative complexes has been previously proposed as an adaptative response to proteasome inhibition, even though the biological role of these assemblies is still unknown[41].
- FaDu cells showed the greatest extent of proteasome loss during treatment, a phenomenon which, to the best of our knowledge, has never been reported in the presence of a proteasome inhibitor. Remarkably, this Bortezomib-induced effect was observed, though to a variable extent, in all human cell lines tested so far, underscoring that it may be a general issue of pharmacological relevance, if confirmed *in vivo*.

For what concerns the proteasome loss, we cannot rule out *a priori* that it is a technical artifact, even though it seems unlikely, since

- the immunostaining was performed with an antibody which targets an epitope shared by 6 out of 7 α-subunits of the proteasome; therefore, it looks unlikely that the residues, which are part of the epitope, undergo post-translational modifications which shield it from antibody recognition in all subunits;
- upon analysis by denaturing and reducing Western Blotting of the same cytosolic extract that was run by native gel electrophoresis, the immunostaining of individual proteasome subunits revealed no

difference at the earliest time-point while at the latest time-point a marked tendency toward increase was observed for all tested cell lines but A-253 cells.

Therefore, this finding envisages that the proteasome loss should not be attributable to the enhanced degradation by macroautophagy (or by other enzymatic pathways) nor to translocation of the particles into other intracellular compartments (*e.g.*, outer surface of ER and nucleus) which are excluded from crude cell extracts preparation. It is then conceivable that Bortezomib inhibition induced a disassembly of proteasome and FaDu cells respond to this insult more quickly than other cell lines, at least *in vitro*.

Overall, our *in vitro* findings suggest that in HNC, showing limited proteasome resistance to Bortezomib and simultaneous upregulation of ErbB receptors-mediated signaling, anti-ErbB receptors antibodies or inhibitors of the ErbB receptors intrinsic tyrosine kinase activity should be used in combination with proteasome inhibitors.

In addition, regarding the analysis of the effects of Bortezomib on experimental models in HNC, there are several studies which have shown that Bortezomib has promising anticancer activities in mouse tumor models[45,46,56,88–90]. However, only two studies analyzed the ability of Bortezomib to counteract the *in vivo* HNC tumor growth, but they were restricted to xenografts implanted human larynx or tongue squamous cell carcinoma cell lines[46,56]. Accordingly, none of them have investigated the *in vivo* effect of Bortezomib in salivary gland carcinoma cell line. Thus, this is the first study showing the *in vitro* and *in vivo* growth inhibitory properties of Bortezomib in a salivary gland carcinoma cell line (SALTO-5) and the *in vivo* effects of Bortezomib on ErbB2, AKT and caspase 3 expression in SALTO-5 cell line transplanted in BALB-*neu*T mice. The Bortezomib effects on SALTO-5 cells were first analyzed *in vitro*. We observed apoptosis and inhibition of ErbB2, p38 and AKT, and activation of JNK in Bortezomib-treated SALTO-5 cell line. In contrast to the human cells analyzed, Bortezomib induced an increase of ERK2 phosphorylation in SALTO-5 cells, which was still associated with the activation of the apoptotic process. On the other hand, regarding the effect of Bortezomib on proteasome, SALTO-5 cells displayed a significant recovery of proteasome particles after 24 hours and of proteasome subunits content associated to a decrease of poly-ubiquitinated proteins. Although the study of apoptosis pathway did not put in evidence any resistance of these cells greater than that of SCC-15, A-253 or CAL-27 cells, it is likely that this mechanisms of resistance to the drug may emerge over a prolonged time of treatment. Cytotoxic and apoptotic effects of Bortezomib in SALTO-5 cell line were also observed by ultrastructural analysis.

In light of the *in vitro* results, we also evaluated the *in vivo* anti-tumor effects of Bortezomib on tumor growth in BALB-*neu*T mice subcutaneously inoculated with syngeneic murine SALTO-5 cells. Several studies have also evaluated the efficacy of Bortezomib in relation to the route of administration, and it has been shown that intraperitoneal (i.p.) administration, at least twice a week, resulted in greater Bortezomib activity with less toxicity[91]. These preclinical investigations have collectively demonstrated the anticancer activity of Bortezomib when used as monotherapy or in combination with chemotherapy, radiotherapy, or other anti-neoplastic agents[91–96].

Our results showed for the first time that intraperitoneal administration of Bortezomib (0.5 mg/kg, twice a week) reduced the growth of SALTO-5 murine cells in mice. The increase in mean survival time of the mice treated with Bortezomib was relevant, as compared to that of the control mice. Furthermore, the growth risk of SALTO-5 cells in control mice is over 13-fold higher than that of Bortezomib-treated mice. In addition, the histological examination of tumors from Bortezomib-treated mice showed extensive necrosis and presence of apoptotic cells, as compared to the control mice. According to the *in vitro* results, the IHC analysis revealed the decrease of the expression of ErbB2 and of the AKT phosphorylation in tumors from Bortezomib-treated mice with respect to control mice. AKT inhibition by Bortezomib *in vivo* was observed in homogenates from tumors of a tongue squamous cell carcinoma cell line transplanted in mice[46]. Our results provide evidence that Bortezomib inhibited *in vivo* the expression of ErbB2 simultaneously to that of AKT. One previous study showed that tumor specimens, from mice transplanted with a human larynx cell line and treated with Bortezomib, displayed cell nuclear condensation and tissue degradation, as well as apoptotic areas[56].

Overall, our results showed that anti-cancer activities of Bortezomib in tongue, pharynx and salivary gland cancer cells were dependent on cell line histotype and associated with the different extent of proteasome inhibition. The inhibition of proteasome was in turn associated with the modulation of the main signaling transduction pathways involved in HNC cellular transformation. Furthermore, for the first time we showed that Bortezomib displayed *in vitro* and an *in vivo* antitumor activity in an adenocarcinoma of the salivary gland. Intraperitoneal administration of Bortezomib interfered with the *in vivo* tumor growth of SALTO-5 cells in BALB-*neu*T mice and prolonged mice median survival time. The inhibition of tumor growth by Bortezomib was associated with tumor necrosis and apoptosis and with the simultaneous inhibition of ErbB2, AKT.

Our *in vitro* and *in vivo* findings further support the use of the proteasome inhibitor Bortezomib for the treatment of HNSCC and adenocarcinomas of the salivary gland and reveal its ineffectiveness in counteracting the activation of deregulated specific signaling pathways in HNC cell lines when resistance to proteasome inhibition is developed, thus suggesting the combined use of Bortezomib and specific drugs targeting signaling transduction pathways unaffected by Bortezomib treatment.

Declarations

Acknowledgments

The authors wish to thank Barbara Bulgarini for help in manuscript preparation. SALTO-5 cells were kindly provided by Prof. F. Cavallo (University of Torino, Italy) and P.L. Lollini (University of Bologna, Italy). Founder male BALB-*neu*T mice were kindly provided by Prof. G. Forni and Prof. F. Cavallo (University of Torino, Italy). S.C. is recipient of the Tor Vergata program in Tissue Engineering and Remodeling Biotechnologies for Body Functions. S.F. is recipient of the Sapienza program in Molecular Medicine.

Author Contributions

Conceptualization, L.M, M.C. and R.B.; formal analysis, M.B., C.F. and D.S.; investigation, M.B., S.C., C.F., S.F., D.S. and L.M; resources, L.M., M.C. and R.B.; writing—original draft preparation, M.B., S.C., D.S., M.C. and R.B.; writing—review and editing, C.F., G.R.T., G.B., M.S., V.M., A.M., L.M. and M.C.; visualization, M.B., D.S. and L.M.; supervision, L.M., M.C. and R.B.; project administration, R.B.; funding acquisition, R.B. All authors have read and agreed to the published version of the manuscript.

Funding

This research was funded by a grant from the University of Rome “Tor Vergata”, Mission Sustainability (Codice Unico di Progetto (CUP): E81I18000330005 to R.B.).

Additional Information

Competing Interests

The authors declare no conflict of interest.

References

1. Chow, L. Q. M. Head and neck cancer. *N. Engl. J. Med.* **382**, 60–72, DOI: https://doi.org/10.1056/NEJMra1715715 (2020).
2. Bray, F. *et al.* Global cancer statistics 2018: GLOBOCAN estimates of incidence and mortality worldwide for 36 cancers in 185 countries. *CA Cancer J. Clin.* **68**, 394–424, DOI: https://doi.org/10.3322/caac.21492 (2018).
3. Joshi, N. P. & Broughman, J. R. Postoperative management of salivary gland tumors. *Curr. Treat. Options Oncol.* **22**, 23, DOI: https://doi.org/10.1007/s11864-021-00820-9 (2021).
4. Bashraheel, S. S., Domling, A. & Goda, S. K. Update on targeted cancer therapies, single or in combination, and their fine tuning for precision medicine. *Biomed. Pharmacother.* **125**, 110009, DOI: https://doi.org/10.1016/j.biopha.2020.110009 (2020).
5. Lee, Y. T., Tan, Y. J. & Oon, C. E. Molecular targeted therapy: treating cancer with specificity. *Eur. J. Pharmacol.* **834**, 188–196, DOI: https://doi.org/10.1016/j.ejphar.2018.07.034 (2018).
6. Kitamura, N. *et al.* Current trends and future prospects of molecular targeted therapy in head and neck squamous cell carcinoma. *Int. J. Mol. Sci.* **22**, 240, DOI: https://doi.org/10.3390/ijms22010240 (2021).
7. Nadhan, R., Srinivas, P. & Pillai M. R. RTKs in pathobiology of head and neck cancers. *Adv. Cancer Res.* **147**, 319–373, DOI: https://doi.org/10.1016/bs.acr.2020.04.008 (2020).
8. Alsahafi, E. *et al.* Clinical update on head and neck cancer: molecular biology and ongoing challenges. *Cell death & disease* **10**, 540, DOI: https://doi.org/10.1038/s41419-019-1769-9 (2019).
9. Harsha, C. *et al.* Targeting AKT/mTOR in oral cancer: mechanisms and advances in clinical trials. *Int. J. Mol. Sci.* **21**, 3285, DOI: https://doi.org/10.3390/ijms21093285 (2020).

10. Vermorken, J. B. *et al.* Platinum-based chemotherapy plus cetuximab in head and neck cancer. *N. Engl. J. Med.* **359**, 1116–1127, DOI: https://doi.org/10.1056/NEJMoa0802656 (2008).
11. Byeon, H. K., Ku, M. & Yang, J. Beyond EGFR inhibition: multilateral combat strategies to stop the progression of head and neck cancer. *Exp. Mol. Med.* **51**, 1–14, DOI: https://doi.org/10.1038/s12276-018-0202-2 (2019).
12. Picon, H. & Guddati, A. K. Mechanisms of resistance in head and neck cancer. *Am. J. Cancer Res.* **10**, 2742–2751 (2020).
13. Roeten, M. S. F., Cloos, J. & Jansen, G. Positioning of proteasome inhibitors in therapy of solid malignancies. *Cancer Chemother. Pharmacol.* **81**, 227–243, DOI: https://doi.org/10.1007/s00280-017-3489-0 (2018).
14. Kisselev, A. F., Van der Linden, W. A., Overkleeft, H. S. Proteasome Inhibitors: an expanding army attacking a unique target. *Chem. Biol.* **19**, 99–115, DOI: https://doi.org/10.1016/j.chembiol.2012.01.003 (2012).
15. Tundo, G. R. *et al*. The proteasome as a druggable target with multiple therapeutic potentialities: cutting and non-cutting edges. *Pharmacol. Ther.* **213**, 107579, DOI: https://doi.org/10.1016/j.pharmthera.2020.107579 (2020).
16. Hershko, A.; Ciechanover, A. & Varshavsky, A. Basic medical research award. The ubiquitin system. *Nat. Med.* **6**, 1073–1081, DOI: https://doi.org/10.1038/80384 (2000).
17. Livneh, I., Cohen-Kaplan, V., Cohen-Rosenzweig, C., Avni, N. & Ciechanover, A. The life cycle of the 26S proteasome: from birth, through regulation and function, and onto its death. *Cell Res.* **26**, 869–885, DOI: https://doi.org/10.1038/cr.2016.86 (2016).
18. Groll, M. *et al.* A gated channel into the proteasome core particle. *Nat. Struct. Biol.* **7**, 1062–1067, DOI: https://doi.org/10.1038/80992 (2000).
19. Raynes, R., Pomatto, L. C. & Davies, K. J. Degradation of oxidized proteins by the proteasome: distinguishing between the 20S, 26S, and immunoproteasome proteolytic pathways. *Mol. Aspects Med.* **50**, 41–55, DOI: https://doi.org/10.1016/j.mam.2016.05.001 (2016).
20. Jackson, G., Einsele, H., Moreau, P. & Miguel, J. S. Bortezomib, a novel proteasome inhibitor, in the treatment of hematologic malignancies. *Cancer Treat. Rev.* **31**, 591–602, DOI: https://doi.org/10.1016/j.ctrv.2005.10.001 (2005).
21. Papandreou, C. N. & Logothetis, C. J. Bortezomib as a potential treatment for prostate cancer. *Cancer Res.* **64**, 5036–5043, DOI: https://doi.org/10.1158/0008-5472.CAN-03-2707 (2004).
22. Kane, R. C., Bross, P. F., Farrell, A. T. & Pazdur, R. Velcade: U.S. FDA approval for the treatment of multiple myeloma progressing on prior therapy. *Oncologist* **8**, 508–513, DOI: https://doi.org/10.1634/theoncologist.8-6-508 (2003).
23. Adams, J. Proteasome inhibitors as new anticancer drugs. *Curr. Opin. Oncol.* **14**, 628–634, DOI: https://doi.org/10.1097/00001622-200211000-00007 (2002).
24. Jagannath, S. *et al.* Bortezomib therapy alone and in combination with dexamethasone for previously untreated symptomatic multiple myeloma. *Br. J. Haematol.* **129**, 776–783, DOI:

https://doi.org/10.1111/j.1365-2141.2005.05540.x (2005).

25. Kondagunta, G. V. *et al.* Phase II trial of bortezomib for patients with advanced renal cell carcinoma. *J. Clin. Oncol.* **22**, 3720–3725, DOI: https://doi.org/10.1200/JCO.2004.10.155 (2004).
26. Shah, S. A. *et al.* 26S proteasome inhibition induces apoptosis and limits growth of human pancreatic cancer. *J. Cell. Biochem.* **82**, 110–122, DOI: https://doi.org/10.1002/jcb.1150 (2001).
27. Chung, C. H. *et al.* Nuclear factor-kappa B pathway and response in a phase II trial of bortezomib and docetaxel in patients with recurrent and/or metastatic head and neck squamous cell carcinoma. *Ann. Oncol.* **21**, 864–870, DOI: https://doi.org/10.1093/annonc/mdp390 (2010).
28. Dudek, A. Z. *et al.* Phase I study of bortezomib and cetuximab in patients with solid tumours expressing epidermal growth factor receptor. *Br. J. Cancer* **100**, 1379–1384, DOI: https://doi.org/10.1038/sj.bjc.6605043 (2009).
29. Davies, A. M. *et al.* Phase I study of two different schedules of bortezomib and pemetrexed in advanced solid tumors with emphasis on non-small cell lung cancer. *J. Thorac. Oncol.* **2**, 1112–1116. DOI: https://doi.org/10.1097/JTO.0b013e31815ba7d0 (2007).
30. Gilbert, J. *et al.* Phase II 2-arm trial of the proteasome inhibitor, PS-341 (bortezomib) in combination with irinotecan or PS-341 alone followed by the addition of irinotecan at time of progression in patients with locally recurrent or metastatic squamous cell carcinoma of the head and neck (E1304): a trial of the Eastern Cooperative Oncology Group. *Head Neck* **35**, 942–948, DOI: https://doi.org/10.1002/hed.23046 (2013).
31. Falchook, G. S. *et al.* Targeting hypoxia-inducible factor-1α (HIF-1α) in combination with antiangiogenic therapy: a phase I trial of bortezomib plus bevacizumab. *Oncotarget* **5**, 10280–10292, DOI: https://doi.org/10.18632/oncotarget.2163 (2014).
32. Argiris, A. *et al.* A phase 2 trial of bortezomib followed by the addition of doxorubicin at progression in patients with recurrent or metastatic adenoid cystic carcinoma of the head and neck: a trial of the eastern cooperative oncology group (E1303). *Cancer* **117**, 3374–3382, DOI: https://doi.org/10.1002/cncr.25852 (2011).
33. Argiris, A. *et al.* Early tumor progression associated with enhanced EGFR signaling with bortezomib, cetuximab, and radiotherapy for head and neck cancer. *Clin. Cancer Res.* **17**, 5755–5764, DOI: https://doi.org/10.1158/1078-0432.CCR-11-0861 (2011).
34. Kubicek, G. J. *et al.* Phase I trial using the proteasome inhibitor bortezomib and concurrent chemoradiotherapy for head-and-neck malignancies. *Int. J. Radiat. Oncol. Biol. Phys.* **83**, 1192–1197, DOI: https://doi.org/10.1016/j.ijrobp.2011.09.023 (2012).
35. Bei, R. *et al.* Colocalization of multiple ErbB receptors in stratified epithelium of oral squamous cell carcinoma. *J Pathol* **195**, 343–348. DOI: https://doi.org/10.1002/path.965 (2001).
36. Rivas, S., Gómez-Oro, C., Antón, I. M., Wandosell, F. Role of Akt isoforms controlling cancer stem cell survival, phenotype and self-renewal. *Biomedicines* **6**, 29, DOI: https://doi.org/10.3390/biomedicines6010029 (2018).

37. Mizushima, N., Yoshimori, T. How to interpret LC3 immunoblotting. *Autophagy* **3**, 542–545. DOI: https://doi.org/10.4161/auto.4600 (2007).
38. Klionski, D. J. *et al*. Guidelines for the use and interpretation of assays for monitoring autophagy (4th edition). *Autophagy* **17**, 1–382, DOI: https://doi.org/10.1080/15548627.2020.1797280 (2021).
39. Bowler, E. *et al*. Pharmacological inhibition of ATR can block autophagy through an ATR-independent mechanism. *iScience* **23**, 101668, DOI: https://doi.org/10.1016/j.isci.2020.101668 (2020).
40. Elsasser, S., Schmidt, M. & Finley, D. Characterization of the proteasome using native gel electrophoresis. *Methods Enzymol.* **398**, 353–363, DOI: https://doi.org/10.1016/S0076-6879(05)98029-4 (2005).
41. Welk, V. *et al.* Inhibition of proteasome activity induces formation of alternative proteasome complexes. *J. Biol. Chem. 291*, 13147–13159, DOI: https://doi.org/10.1074/jbc.M116.717652 (2016).
42. Adams J. The proteasome: structure, function, and role in the cell. *Cancer Treat. Rev.* **29 Suppl 1**, 3–9, DOI: https://doi.org/10.1016/s0305-7372(03)00081-1 (2003).
43. Adams, J. *et al.* Proteasome inhibitors: a novel class of potent and effective antitumor agents. *Cancer Res.* **59**, 2615–2622 (1999).
44. Shanker, A. *et al.* Treating metastatic solid tumors with bortezomib and a tumor necrosis factor-related apoptosis-inducing ligand receptor agonist antibody. *J. Natl. Cancer Inst.* **100**, 649–662, DOI: https://doi.org/10.1093/jnci/djn113 (2008).
45. Sunwoo, J. B. *et al.* Novel proteasome inhibitor PS-341 inhibits activation of nuclear factor-κB, cell survival, tumor growth and angiogenesis in squamous cell carcinoma. *Clin. Cancer Res.* **7**, 1419–1428 (2001).
46. Lin, Y. C., Chen, K. C., Chen, C. C., Cheng, A. L. & Chen, K. F. CIP2A-mediated Akt activation plays a role in bortezomib-induced apoptosis in head and neck squamous cell carcinoma cells. *Oral Oncol.* **48**, 585–593, DOI: https://doi.org/10.1016/j.oraloncology.2012.01.012 (2012).
47. Li, C. & Johnson, D. E. Liberation of functional p53 by proteasome inhibition in human papilloma virus-positive head and neck squamous cell carcinoma cells promotes apoptosis and cell cycle arrest. *Cell Cycle* **12**, 923–934, DOI: https://doi.org/10.4161/cc.23882 (2012).
48. Ow, T. J. *et al*. Apoptosis signaling molecules as treatment targets in head and neck squamous cell carcinoma. *Laryngoscope* **130**, 2643–2649, DOI: https://doi.org/10.1002/lary.28441 (2020).
49. Li, C., Li, R., Grandis, J. R. & Johnson, D. E. Bortezomib induces apoptosis via Bim and Bik up-regulation and synergizes with cisplatin in the killing of head and neck squamous cell carcinoma cells. *Mol. Cancer Ther.* **7**, 1647–1655, DOI: https://doi.org/10.1158/1535-7163.MCT-07-2444 (2008).
50. Bullenkamp, J. *et al*. Bortezomib sensitises TRAIL-resistant HPV-positive head and neck cancer cells to TRAIL through a caspase-dependent, E6-independent mechanism. *Cell Death Dis.* **5**, e1489, DOI: https://doi.org/10.1038/cddis.2014.455 (2014).
51. Fribley, A., Zeng, Q. & Wang, C. Y. Proteasome inhibitor PS-341 induces apoptosis through induction of endoplasmic reticulum stress-reactive oxygen species in head and neck squamous cell carcinoma

cells. *Mol. Cell. Biol.* **24**, 9695–9704, DOI: https://doi.org/10.1128/MCB.24.22.9695-9704.2004 (2004).

52. Kim, J. *et al*. PS-341 and histone deacetylase inhibitor synergistically induce apoptosis in head and neck squamous cell carcinoma cells. *Mol. Cancer Ther.* **9**, 1977–1984, DOI: https://doi.org/10.1158/1535-7163.MCT-10-0141 (2010).
53. Wagenblast, J. *et al*. Effects of combination treatment of bortezomib and dexamethasone in SCCHN cell lines depend on tumor cell specificity. *Oncol. Rep.* **20**, 1207–1211 (2008).
54. Leinung, M. *et al*. Fighting cancer from different signaling pathways: Effects of the proteasome inhibitor Bortezomib in combination with the polo-like-kinase-1-inhibitor BI2536 in SCCHN. *Oncol. Lett.* **4**, 1305–1308, DOI: https://doi.org/10.3892/ol.2012.927 (2012).
55. Li, C. V. *et al.* Bortezomib up-regulates activated signal transducer and activator of transcription-3 and synergizes with inhibitors of signal transducer and activator of transcription-3 to promote head and neck squamous cell carcinoma cell death. *Mol. Cancer Ther.* **8**, 2211–2220, DOI: https://doi.org/10.1158/1535-7163.MCT-09-0327 (2009).
56. Chen, Z. *et al.* Differential bortezomib sensitivity in head and neck cancer lines corresponds to proteasome, nuclear factor-kappaB and activator protein-1 related mechanisms. *Mol. Cancer Ther.* **7**, 1949–1960, DOI: https://doi.org/10.1158/1535-7163.MCT-07-2046 (2008).
57. Wagenblast, J., Hambek, M., Baghi, M. & Knecht, R. Effect of bortezomib on EGFR expression in head and neck squamous cell carcinoma cell lines. *Anticancer Res.* **28**, 687–692 (2008).
58. Li, C. & Johnson, D. E. Bortezomib induces autophagy in head and neck squamous cell carcinoma cells via JNK activation. *Cancer Lett.* **314**, 102–107, DOI: https://doi.org/10.1016/j.canlet.2011.09.020 (2012).
59. Chang, I. & Wang, C. Y. Inhibition of HDAC6 protein enhances bortezomib-induced apoptosis in head and neck squamous cell carcinoma (HNSCC) by reducing autophagy. *J. Biol. Chem.* **291**, 18199–18209, DOI: https://doi.org/10.1074/jbc.M116.717793 (2016).
60. Weber, C. N., Cerniglia, G. J., Maity, A. & Gupta, A. K. Bortezomib sensitizes human head and neck carcinoma cells SQ20B to radiation. *Cancer Biol. Ther.* **6**, 156–159, DOI: https://doi.org/10.4161/cbt.6.2.3556 (2007).
61. Di Villeneuve, L., Souza, I. L., Tolentino, F. D. S., Ferrarotto, R. & Schvartsman, G. Salivary gland carcinoma: novel targets to overcome treatment resistance in advanced disease. *Front. Oncol.* 2020, *10*, 580141, DOI: https://doi.org/10.3389/fonc.2020.580141 (2020).
62. Vattemi, E. *et al*. Systemic therapies for recurrent and/or metastatic salivary gland cancers. *Expert Rev. Anticancer Ther.* **8**, 393–402, DOI: https://doi.org/10.1586/14737140.8.3.393 (2008).
63. Andry, G., Hamoir, M., Locati, L. D., Licitra, L. & Langendijk, J. A. Management of salivary gland tumors. *Expert Rev. Anticancer Ther.* **12**, 1161–1168, DOI: https://doi.org/10.1586/era.12.92 (2012).
64. Hong, Y. S. *et al*. Bortezomib induces G2-M arrest in human colon cancer cells through ROS-inducible phosphorylation of ATM-CHK1. *Int. J. Oncol.* **41**, 76–82, DOI: https://doi.org/10.3892/ijo.2012.1448 (2012).

65. Ling, Y. H. *et al*. Mechanisms of proteasome inhibitor PS-341-induced G(2)-M-phase arrest and apoptosis in human non-small cell lung cancer cell lines. *Clin. Cancer Res.* **9**, 1145–1154 (2003).

66. Lu, G., Punj, V. & Chaudhary, P. M. Proteasome inhibitor Bortezomib induces cell-cycle arrest and apoptosis in cell lines derived from Ewing's sarcoma family of tumors and synergizes with TRAIL. *Cancer Biology & Therapy* **7**, 603–608, DOI: https://doi.org/10.4161/cbt.7.4.5564 (2008).

67. Wang, Y. *et al*. Targeted proteasome inhibition by Velcade induces apoptosis in human mesothelioma and breast cancer cell lines. *Cancer Chemother. Pharmacol.* **66**, 455–466, DOI: https://doi.org/10.1007/s00280-009-1181-8 (2010).

68. Bei, R. *et al*. Frequent overexpression of multiple ErbB receptors by head and neck squamous cell carcinoma contrasts with rare antibody immunity in patients. *J. Pathol.* **204**, 317–325, DOI: https://doi.org/10.1002/path.1642 (2004).

69. Xia, W. *et al*. Combination of EGFR, HER-2/neu, and HER-3 is a stronger predictor for the outcome of oral squamous cell carcinoma than any individual family members. *Clin. Cancer Res.* **5**, 4164–4174 (1999).

70. Graus-Porta, D., Beerli, R. R., Daly, J. M. & Hynes, N. E. ErbB-2, the preferred heterodimerization partner of all ErbB receptors, is a mediator of lateral signaling. *EMBO J.* **16**, 1647–1655, DOI: https://doi.org/10.1093/emboj/16.7.1647 (1997).

71. Masuelli, L. *et al.* In vitro and in vivo anti-tumoral effects of the flavonoid apigenin in malignant mesothelioma. *Front. Pharmacol.* **8**, 373, DOI: https://doi.org/10.3389/fphar.2017.00373 (2017).

72. Masuelli, L. *et al*. Curcumin blocks autophagy and activates apoptosis of malignant mesothelioma cell lines and increases the survival of mice intraperitoneally transplanted with a malignant mesothelioma cell line. *Oncotarget* **8**, 34405–34422, DOI: https://doi.org/10.18632/oncotarget.14907 (2017).

73. Buscà, R., Pouysségur, J. & Lenormand, P. ERK1 and ERK2 Map kinases: specific roles or functional redundancy? *Front. Cell Dev. Biol.* **4**, 53, doi: https://doi.org/10.3389/fcell.2016.00053 (2016).

74. Cagnol, S. & Chambard, J. C. ERK and cell death: mechanisms of ERK induced cell death-apoptosis, autophagy and senescence. *FEBS J.* **277**, 2–21, DOI: https://doi.org/10.1111/j.1742-4658.2009.07366.x (2010).

75. Wada, T. & Penninger, J. M. Mitogen-activated protein kinases in apoptosis regulation. *Oncogene* **23**, 2838–2849, DOI: https://doi.org/10.1038/sj.onc.1207556 (2004).

76. Lei, Y. Y., Wang, W. J., Mei, J. H., Wang, C. L. Mitogen-activated protein kinase signal transduction in solid tumors. *Asian Pac. J. Cancer Prev.* **15**, 8539–8548, DOI: https://doi.org/10.7314/APJCP.2014.15.20.8539 (2014).

77. Lioni, M. *et al.* Bortezomib induces apoptosis in esophageal squamous cell carcinoma cells through activation of the p38 mitogen-activated protein kinase pathway. *Mol. Cancer Ther.* **7**, 2866–2875, DOI: https://doi.org/10.1158/1535-7163.MCT-08-0391 (2008).

78. Yan, H. *et al*. Arsenic trioxide and proteasome inhibitor bortezomib synergistically induce apoptosis in leukemic cells: the role of protein kinase C delta. *Leukemia* **21**, 1488–1495, DOI:

https://doi.org/10.1038/sj.leu.2404735 (2007).

79. Tournier, C. The 2 faces of JNK signaling in cancer. *Genes Cancer* **4**, 397–400, DOI: https://doi.org/10.1177/1947601913486349 (2013).
80. Hideshima, T. *et al.* Molecular mechanisms mediating antimyeloma activity of proteasome inhibitor PS-341. *Blood* **101**, 1530–1534, DOI: https://doi.org/10.1182/blood-2002-08-2543 (2003).
81. Chauhan, D. *et al.* Targeting mitochondria to overcome conventional and bortezomib/proteasome inhibitor PS-341 resistance in multiple myeloma (MM) cells. *Blood* **104**, 2458–2466, DOI: https://doi.org/10.1182/blood-2004-02-0547 (2004).
82. Yang, Y. *et al*. Proteasome inhibitor PS-341 induces growth arrest and apoptosis of non-small cell lung cancer cells via the JNK/c-Jun/AP-1 signaling. *Cancer Sci.* **95**, 176–180, DOI: https://doi.org/10.1111/j.1349-7006.2004.tb03200.x (2004).
83. Kao, C. *et al.* Bortezomib enhances cancer cell death by blocking the autophagic flux through stimulating ERK phosphorylation. *Cell Death Dis.* **5**, e1510, DOI: https://doi.org/10.1038/cddis.2014.468 (2014).
84. Periyasamy-Thandavan S. *et al*. Bortezomib blocks the catabolic process of autophagy via a cathepsin-dependent mechanism, affects endoplasmic reticulum stress and induces caspase-dependent cell death in antiestrogen-sensitive and resistant ER + breast cancer cells. *Autophagy* **6**, 19–35, DOI: https://doi.org/10.4161/auto.6.1.10323 (2010).
85. Armstrong J. L. *et al*. Oncogenic B-RAF signaling in melanoma impairs the therapeutic advantage of autophagy inhibition. *Clin Cancer Res* **17**, 2216–2226. DOI: https://doi.org/10.1158/1078-0432.CCR-10-3003 (2011).
86. Restuccia, D. F. & Hemmings, B. A. From man to mouse and back again: advances in defining tumor AKTivities in vivo. *Dis. Model. Mech.* **3**, 705–720, DOI: https://doi.org/10.1242/dmm.004671 (2010).
87. Tsvetkov, P. *et al*. Compromising the 19S proteasome complex protects cells from reduced flux through the proteasome. *Elife* **4**, e08467, DOI: https://doi.org/10.7554/eLife.08467 (2015).
88. LeBlanc, R. *et al*. Proteasome inhibitor PS-341 inhibits human myeloma cell growth in vivo and prolongs survival in a murine model. *Cancer Res.* **62**, 4996–5000 (2002).
89. Tan, C. & Waldmann, T. A. Proteasome inhibitor PS-341, a potential therapeutic agent for adult T-cell leukemia. *Cancer Res.* **62**, 1083–1086 (2002).
90. Amiri, K. I., Horton, L. W., LaFleur, B. J., Sosman, J. A. & Richmond, A. Augmenting chemosensitivity of malignant melanoma tumors via proteasome inhibition: implication for bortezomib (VELCADE, PS-341) as a therapeutic agent for malignant melanoma. *Cancer Res.* **64**, 4912–4918, DOI: https://doi.org/10.1158/0008-5472.CAN-04-0673 (2004).
91. Boccadoro, M., Morgan, G. & Cavenagh, J. Preclinical evaluation of the proteasome inhibitor bortezomib in cancer therapy. *Cancer Cell Int.* **5**, 18, DOI: https://doi.org/10.1186/1475-2867-5-18 (2005).
92. Wang, S. *et al.* Leucovorin enhances the anti-cancer effect of bortezomib in colorectal cancer cells. *Sci. Rep.* **7**, 682, DOI: https://doi.org/10.1038/s41598-017-00839-9 (2017).

93. Adams, J. The development of proteasome inhibitors as anticancer drugs. *Cancer Cell* **5**, 417–421, DOI: https://doi.org/10.1016/s1535-6108(04)00120-5 (2004).
94. Mitsiades, N. *et al*. The proteasome inhibitor PS-341 potentiates sensitivity of multiple myeloma cells to conventional chemotherapeutic agents: therapeutic applications. *Blood*, **101**, 2377–2380, DOI: https://doi.org/10.1182/blood-2002-06-1768 (2003).
95. Hideshima, T. *et al.* The proteasome inhibitor PS-341 inhibits growth, induces apoptosis, and overcomes drug resistance in human multiple myeloma cells. *Cancer Res.* **61**, 3071–3076, (2001).
96. Ma, M. H. *et al*. The proteasome inhibitor PS-341 markedly enhances sensitivity of multiple myeloma tumor cells to chemotherapeutic agents. *Clin. Cancer Res.* **9**, 1136–1144, (2003).
97. Pannellini, T. *et al*. Timely DNA vaccine combined with systemic IL-12 prevents parotid carcinomas before a dominant-negative p53 makes their growth independent of HER-2/neu expression. *J. Immunol.* **176**, 7695–7703, DOI: https://doi.org/10.4049/jimmunol.176.12.7695 (2006).
98. Benvenuto, M. *et al.* In vitro and in vivo inhibition of breast cancer cell growth by targeting the Hedgehog/GLI pathway with SMO (GDC-0449) or GLI (GANT-61) inhibitors. *Oncotarget*, **7**, 9250–9270, DOI: https://doi.org/10.18632/oncota rget.7062 (2016).
99. Strober, W. Trypan blue exclusion test of cell viability. *Curr. Protoc. Immunol.* **111**, A.3B.1–A.3B.2, DOI: https://doi.org/10.1002/0471142735.ima03bs111 (2015).
100. Benvenuto, M. *et al*. Effect of the BH3 mimetic polyphenol (–)-gossypol (AT-101) on the in vitro and in vivo growth of malignant mesothelioma. *Front. Pharmacol.* **9**, 1269, DOI: https://doi.org/10.3389/fphar.2018.01269 (2018).
101. Masuelli, L. *et al.* In vivo and in vitro inhibition of osteosarcoma growth by the pan Bcl-2 inhibitor AT-101. *Invest. New Drugs*, **38**, 675–689, DOI: https://doi.org/10.1007/s10637-019-00827-y (2020).
102. Masuelli, L. *et al.* Resveratrol potentiates the in vitro and in vivo anti-tumoral effects of curcumin in head and neck carcinomas. *Oncotarget*, **5**, 10745–10762, DOI: https://doi.org/10.18632/oncotarget.2534 (2014).
103. Alesiani, D., Cicconi, R., Mattei, M., Bei, R. & Canini, A. Inhibition of Mek 1/2 kinase activity and stimulation of melanogenesis by 5,7-dimethoxycoumarin treatment of melanoma cells. *In.t J. Oncol.* **34**, 1727–1735, DOI: https://doi.org/10.3892/ijo_00000303 (2009).
104. Sbardella, D. *et al.* The insulin-degrading enzyme is an allosteric modulator of the 20S proteasome and a potential competitor of the 19S. *Cell. Mol. Life Sci.* **75**, 3441–3456, DOI: https://doi.org/10.1007/s00018-018-2807-y (2018).
105. Rovero, S. *et al.* DNA vaccination against rat her-2/Neu p185 more effectively inhibits carcinogenesis than transplantable carcinomas in transgenic BALB/c mice. *J. Immunol.* **165**, 5133–5142, DOI: https://doi.org/10.4049/jimmunol.165.9.5133 (2000).
106. Frajese, G. V. *et al.* Electrochemically reduced water delays mammary tumors growth in mice and inhibits breast cancer cells survival in vitro. *Evid. Based Complement. Alternat. Med.* 2018, 4753507, DOI: https://doi.org/10.1155/2018/4753507 (2018).

107. Masuelli, L. *et al*. Gene-specific inhibition of breast carcinoma in BALB-*neu*T mice by active immunization with rat Neu or human ErbB receptors. *Int. J. Oncol.* **30**, 381–392 (2007).

108. Focaccetti, C. *et al.* Curcumin enhances the antitumoral effect induced by the recombinant vaccinia neu vaccine (rV-neuT) in mice with transplanted salivary gland carcinoma cells. *Nutrients*, **12**, 1417, DOI: https://doi.org/10.3390/nu12051417 (2020).

109. Masuelli, L. *et al.* Local delivery of recombinant vaccinia virus encoding for neu counteracts growth of mammary tumors more efficiently than systemic delivery in neu transgenic mice. *Cancer Immunol. Immunother.* **59**, 1247–1258, DOI: https://doi.org/10.1007/s00262-010-0850-0 (2010).

110. Benvenuto, M. *et al.* Natural humoral immune response to ribosomal P0 protein in colorectal cancer patients. *J. Transl. Med.* **13**, 101, DOI: https://doi.org/10.1186/s12967-015-0455-7 (2015).

111. Masuelli, L. *et al.* Chloroquine supplementation increases the cytotoxic effect of curcumin against Her2/neu overexpressing breast cancer cells in vitro and in vivo in nude mice while counteracts it in immune competent mice. *Oncoimmunology*, **6**, 1356151, DOI: https://doi.org/10.1080/2162402X.2017.1356151 (2017).

Figures

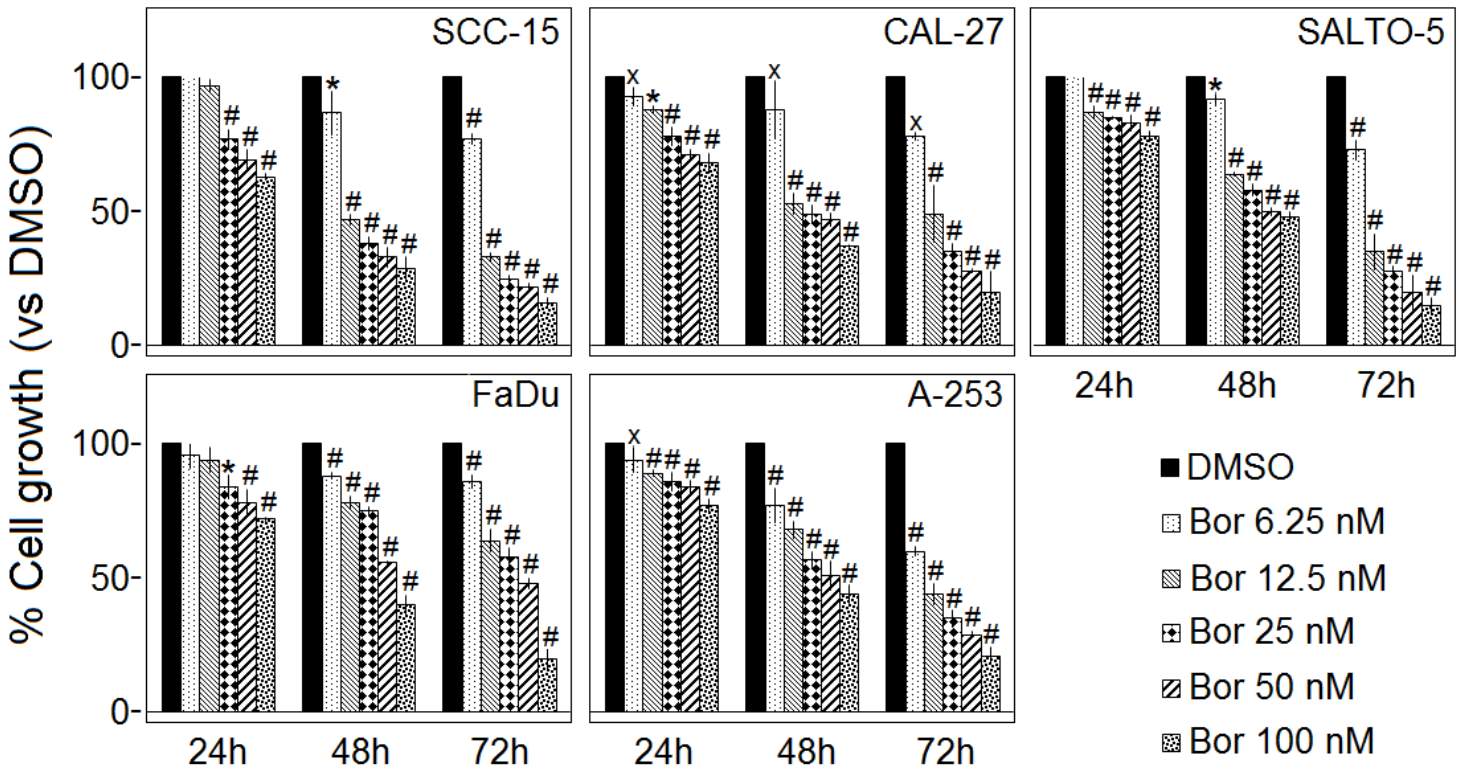

Figure 1

Effect of Bortezomib on the proliferation of carcinoma cell lines of the pharynx (FaDu), tongue (SCC-15, CAL-27) and salivary gland (A-253, SALTO-5). The growth rate of human (SCC-15, CAL-27, FaDu, A-253) and murine (SALTO-5) HNC cell lines was assessed by the SRB assay after 24, 48 and 72 hours of

treatment with DMSO or Bortezomib (Bor). The growth rate of cells treated with Bortezomib was calculated in comparison with that of control cells treated with DMSO. The results are expressed as the mean ± SD of three independent experiments performed in triplicate (xp≤0.05, *p≤0.01, #p≤0.001 vs DMSO).

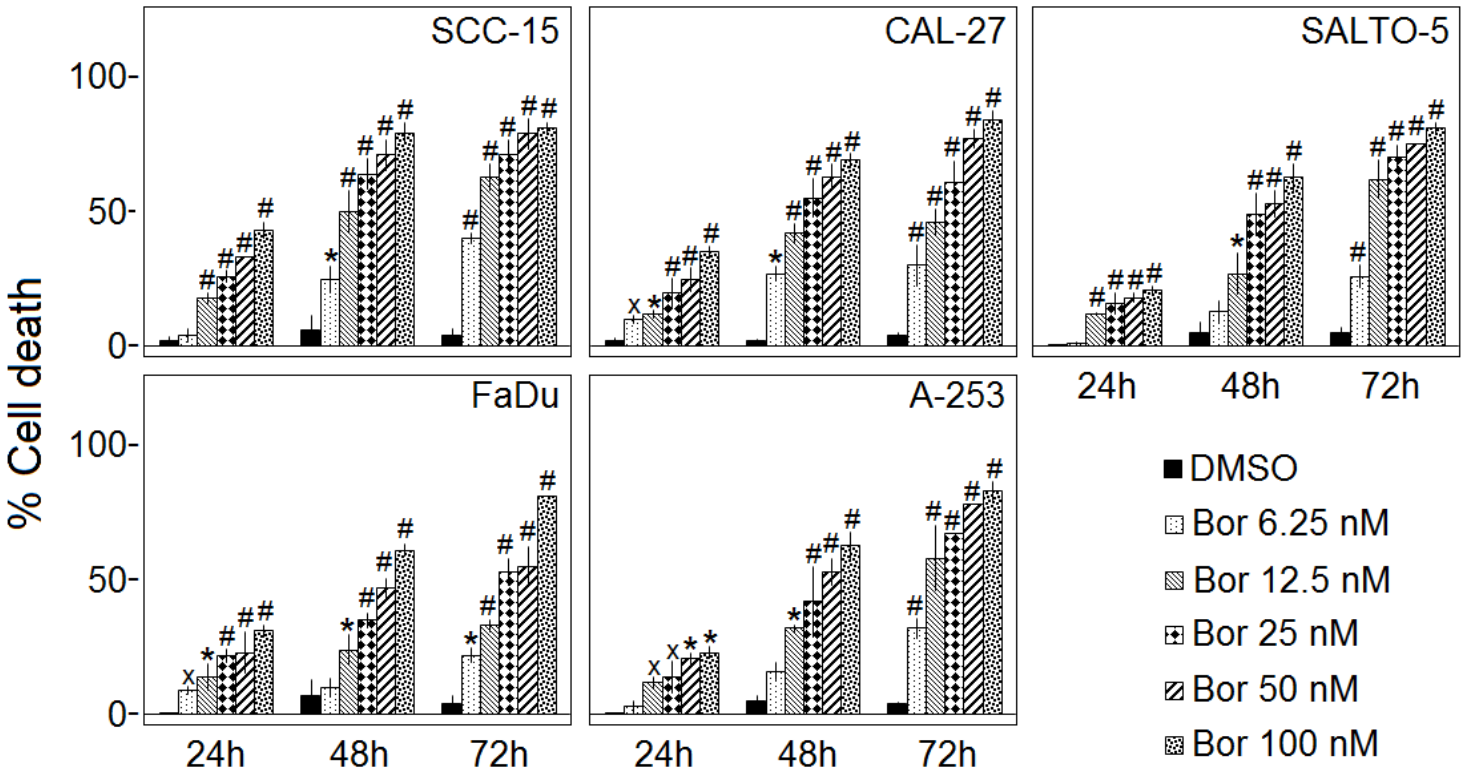

Figure 2

Effect of Bortezomib on the death of the pharynx (FaDu), tongue (SCC-15, CAL-27) and salivary gland (A-253, SALTO-5) cancer cells. The Trypan Blue assay was performed to determine the death rate of HNC cells treated with Bortezomib (Bor) or DMSO after 24, 48 and 72 hours after treatment. Results represent the mean ± SD of three independent experiments performed in triplicate (p ≤ 0.05, *p ≤ 0.01, #p ≤ 0.001 vs DMSO).

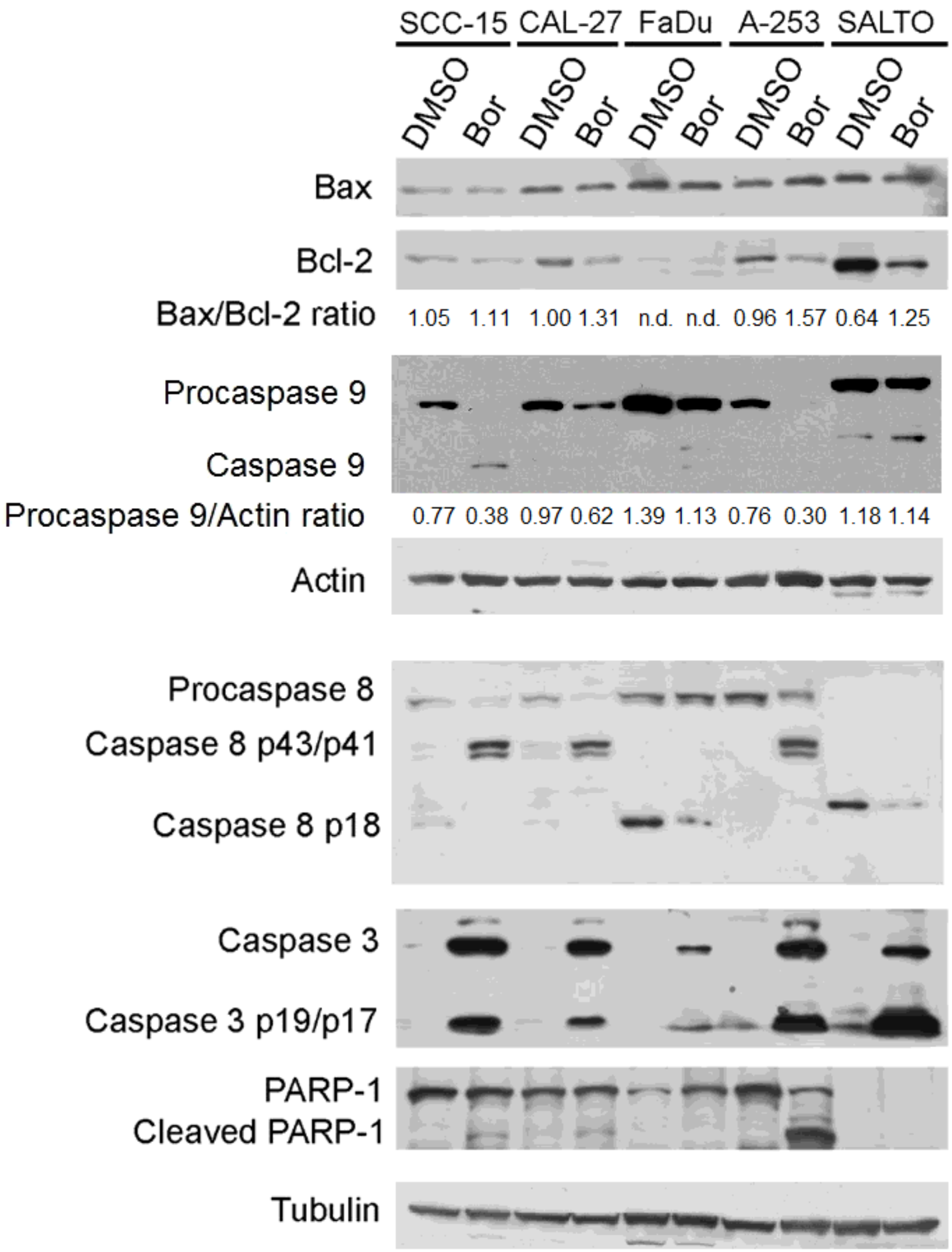

Figure 3

Effect of Bortezomib on the expression of molecules involved in apoptosis in pharynx (FaDu), tongue (SCC-15, CAL-27) and salivary gland (A-253, SALTO-5) cancer cell lines. The expression of Bax, Bcl-2, caspase 9, 8, 3, and PARP-1 was evaluated by Western blotting analysis following treatment for 24 or 48 hours of HNC cells with Bortezomib (Bor) at a dose of 12.5 (SCC-15, CAL-27) or 25 nM or with DMSO, as reported in Materials and Methods. Actin and tubulin were used as an internal control. The reported

"ratios" represent the averages of two experiments. n.d.: not detectable. Uncropped western blots are reported in Supplementary Informations.

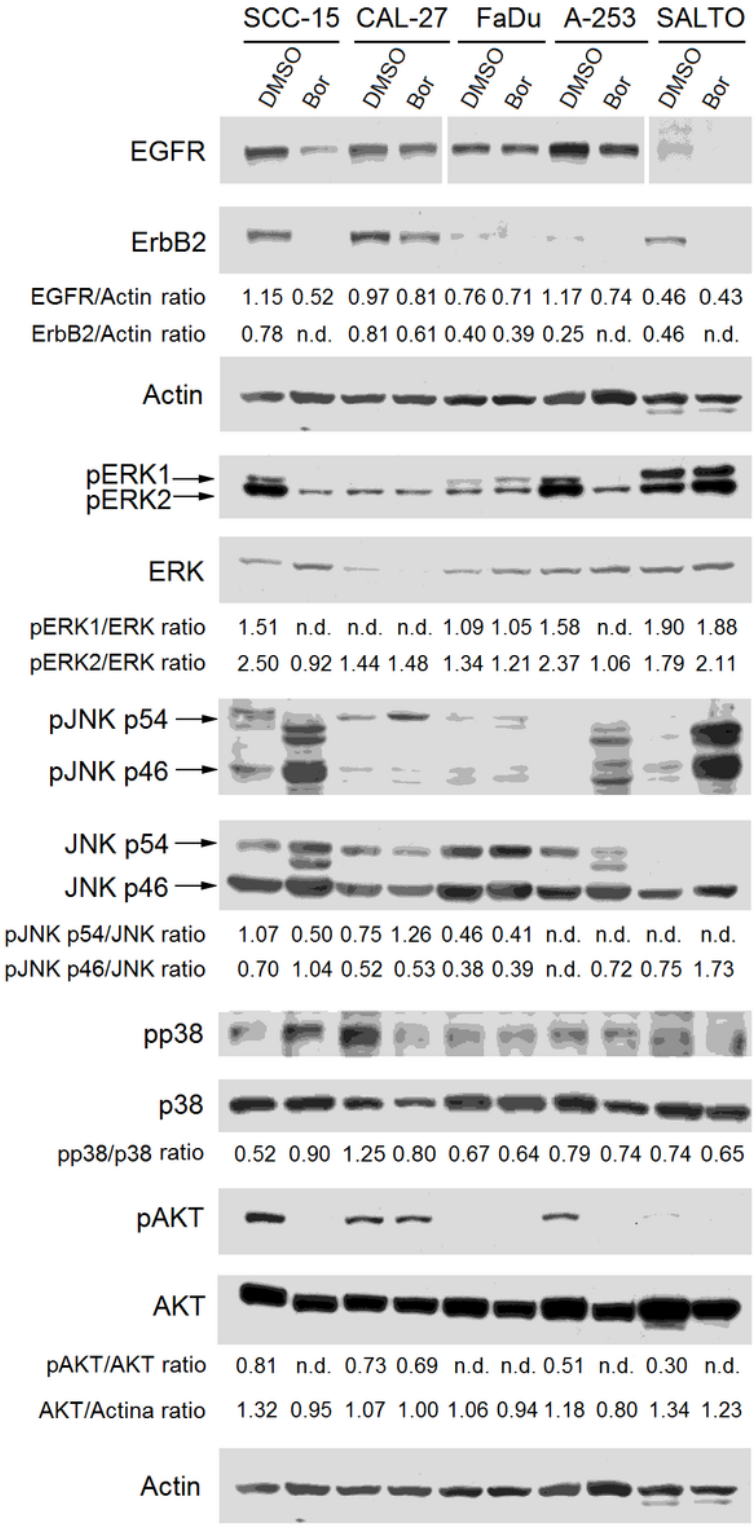

Figure 4

Effect of Bortezomib on the expression and activation of ErbB receptors (EGFR and ErbB2) and signaling transduction pathway molecules. Western blotting analysis was performed on HNC cells treated with Bortezomib (Bor) or DMSO for 24 or 48 hours, at a dose of 12.5 (SCC-15, CAL-27) or 25 nM, as reported in

Materials and Methods. The levels of pERK1, pERK2, pp38, pJNK, as well as pAKT, were compared with that of total ERK, p38, JNK, and AKT proteins, respectively. The intensity of the bands was quantified using the ImageJ software after blot scanning of two independent experiments. The ratios are reported. Actin was used as an internal control. n.d.: not detectable. Uncropped western blots are reported in Supplementary Informations.

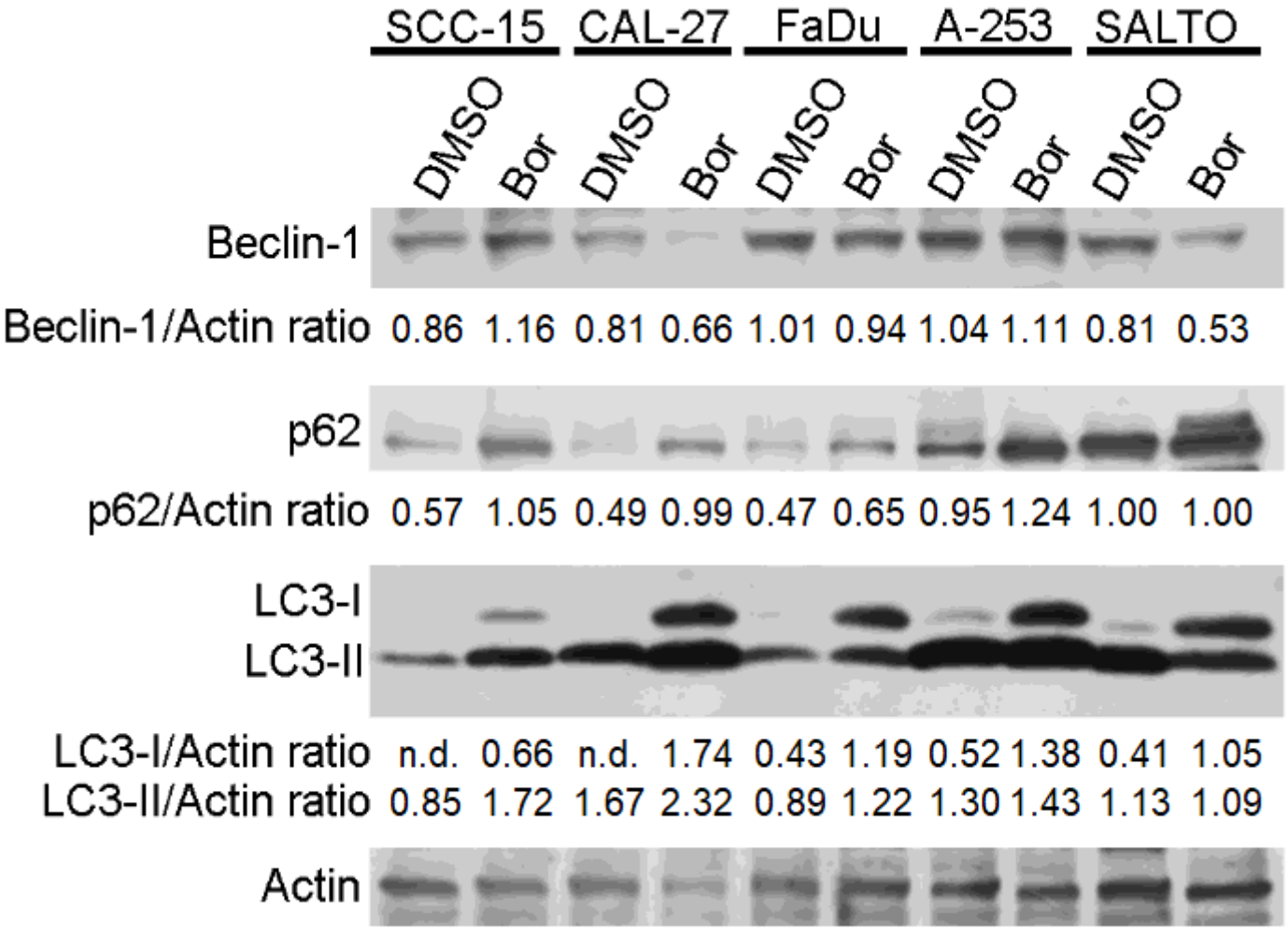

Figure 5

Effect of Bortezomib on autophagy in HNC cells. Western blotting analysis was performed on HNC cells treated with Bortezomib (Bor) or DMSO for 24 or 48 hours, at the dose of 12.5 (SCC-15, CAL-27) or 25 nM, as reported in Materials and Methods. Actin was used as an internal control. The intensity of the bands was quantified using the ImageJ software after blot scanning of two independent experiments. The densitometric ratios between Beclin-1 and actin, p62 and actin, LC3-I and actin, LC3-II and actin are reported. n.d.: not detectable. Uncropped western blots are reported in Supplementary Informations.

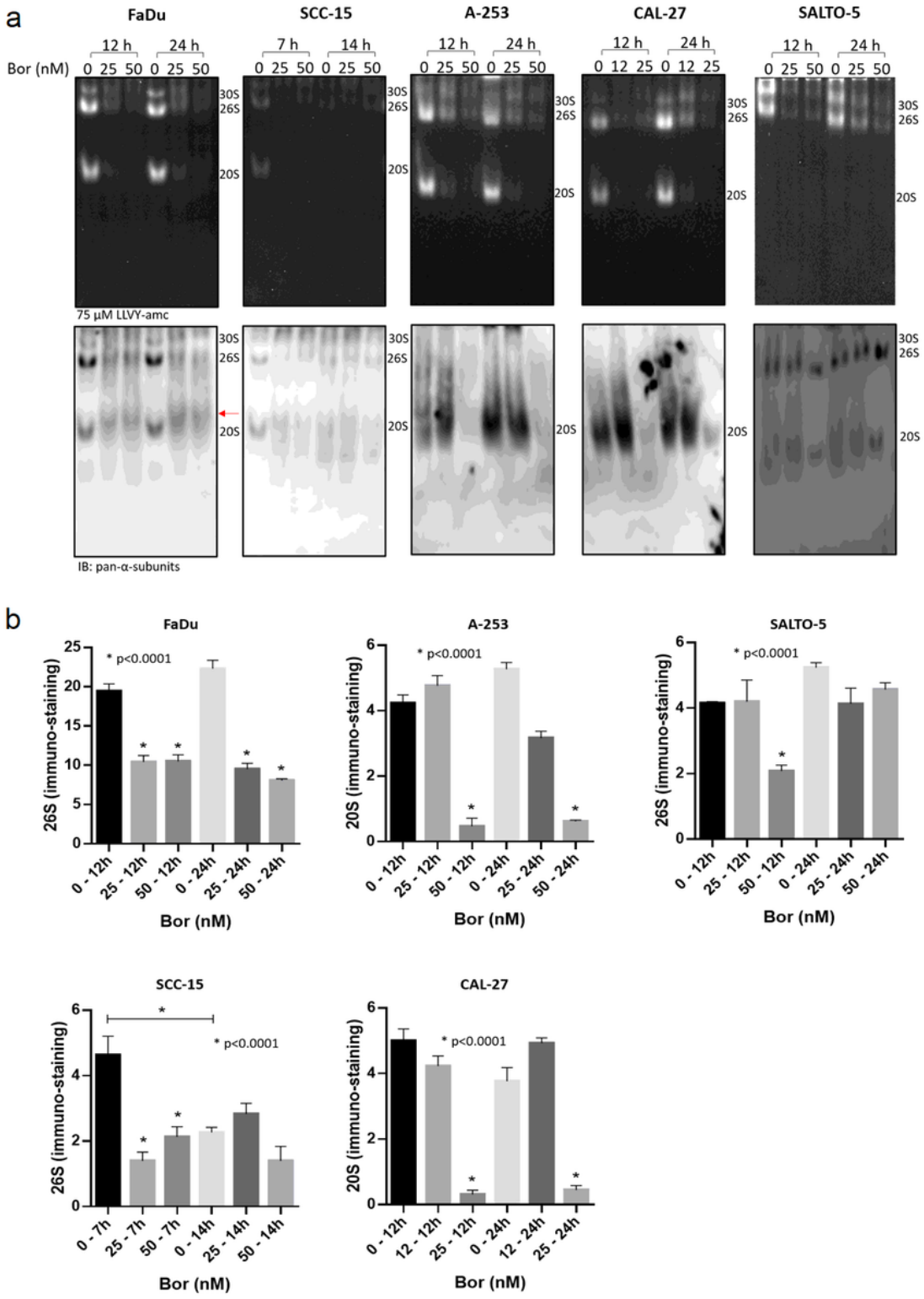

Figure 6

Analysis of structural and functional properties of proteasome particles in the presence of Bortezomib by native-gel electrophoresis coupled with Western blotting. (A) Proteasome particles were separated by native-gel electrophoresis and probed with 75 µM LLVY-amc (upper panel). The light intensity has a linear correlation with the in gel peptidolytic activity. The identity of the particles has been probed with an anti-pan-α-subunits antibody (bottom panel). The red arrow indicates the appearance of non-canonical

proteasome assemblies in FaDu cells treated with Bortezomib (Bor) (bottom panel). (B) Proteasome content was calculated by determining the intensity of the 26S immunostaining for FaDu, SCC-15, SALTO-5 cells and of the 20S for A-253 and CAL-27, that is the most represented species for each cell line assayed. A representative panel of a single experiment is shown. Every assay has been carried out three independent times. Data are presented as mean±SD (n=3). One-way ANOVA followed by Tukey's post-hoc significance test. The reported statistical analysis refers to the ratio between each Bortezomib-related experimental condition vs untreated cells at the same time-point.

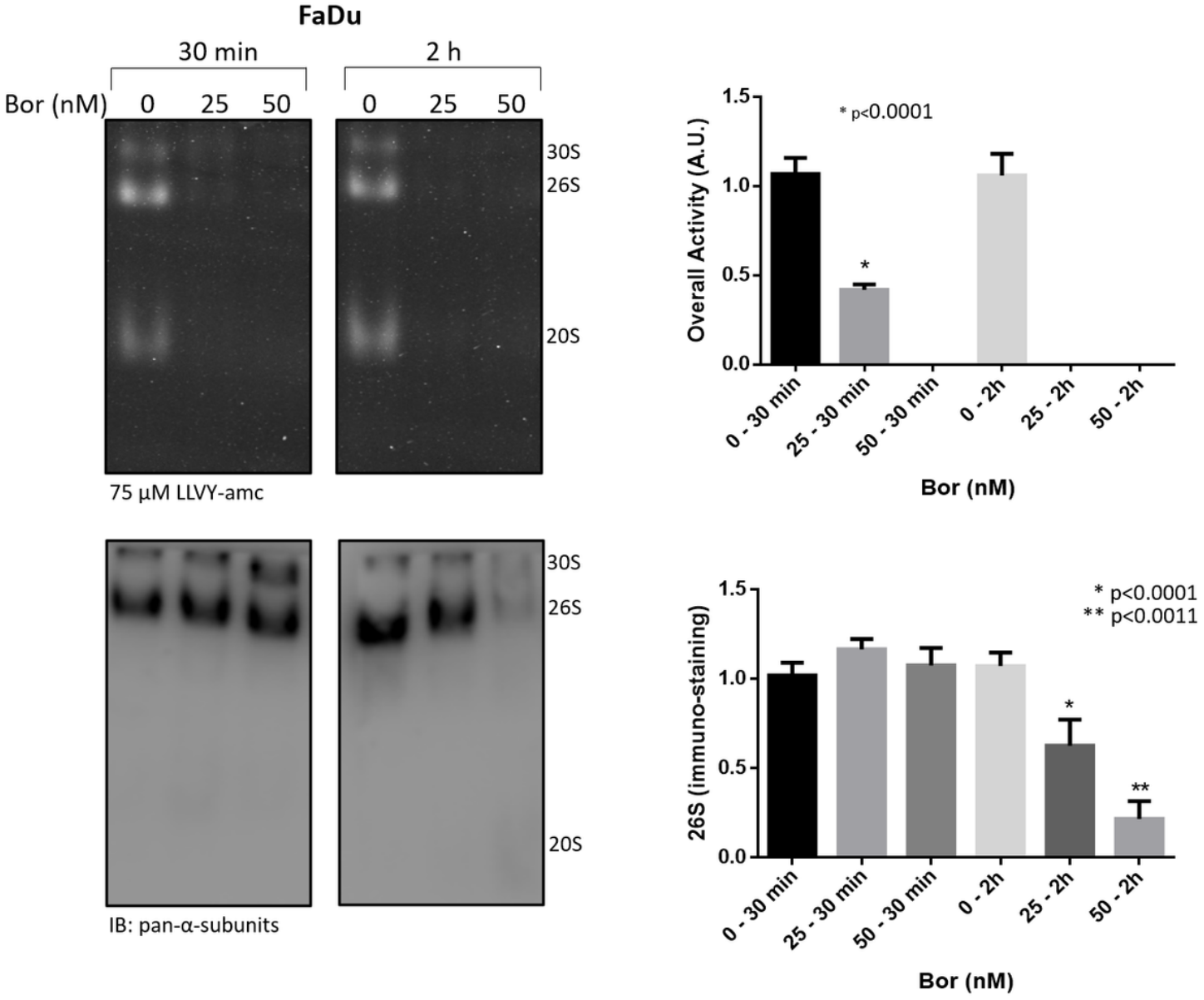

Figure 7

Analysis of proteasome particles at early times after Bortezomib stimulation in FaDu cell line. FaDu cells were treated with 25 and 50 nM Bortezomib (Bor) for 30 minutes and 2 hours and analyzed as described previously by native-gel electrophoresis followed by Western Blotting (left panel). Densitometric analysis of proteasome particles activity was determined by in-gel peptidolytic activity and that of proteasome

immunostaining by Western Blotting (right panel). A representative panel of a single experiment is shown. Every assay has been carried out three independent times. Data are presented as mean±SD (n=3). One-way ANOVA followed by Tukey's post-hoc significance test. The reported statistical analysis refers to the ratio between each Bortezomib-related experimental condition vs untreated cells at the same time-point.

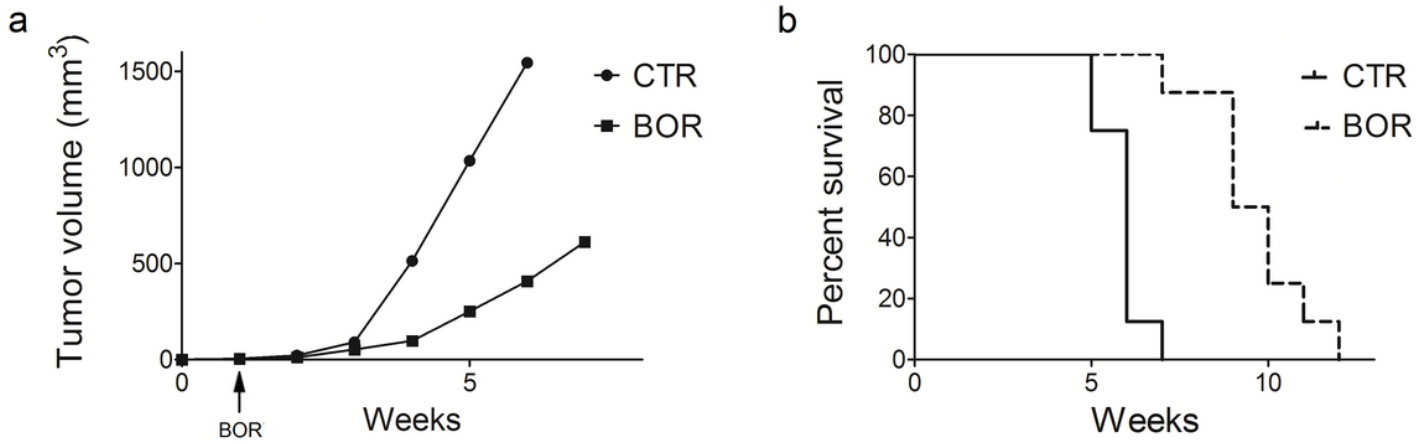

Figure 8

Bortezomib reduced tumor growth and increased the survival in BALB-neuT mice that were subcutaneously inoculated with SALTO-5 cells. (A) Differences in mean tumor volumes between BALB-neuT mice treated with Bortezomib (Bor) or PBS+DMSO (Ctr). (B) Differences in the mean survival duration of BALB-neuT mice treated with Bortezomib (Bor) or PBS+DMSO (Ctr).

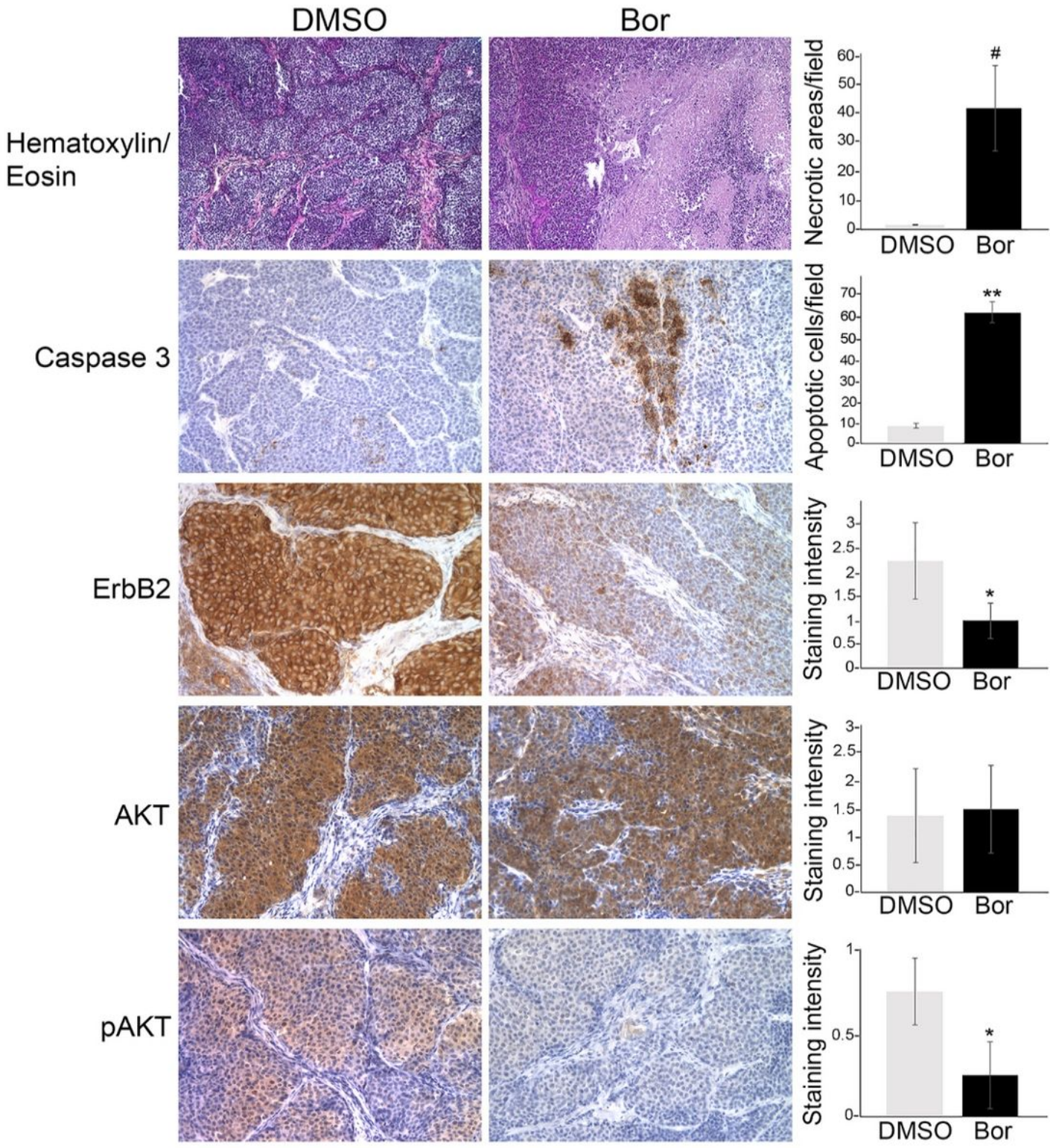

Figure 9

Histology and immunohistochemical analysis of tumors from Bortezomib-treated mice (Bor) or control-treated mice (DMSO). Tumors from three different mice for each group were stained using hematoxylin and eosin. Necrotic areas were quantified by ImageJ software on 10 representative microscopic fields. Percentage average of necrotic areas are reported in the graph. Immunohistochemical analysis was performed to analyse the expression of cleaved caspase 3, ErbB2, AKT and phospho-AKT (pAKT) in

tumor samples. Tumor tissues from three mice in each group were analysed and representative images were reported. The number of cleaved caspase 3-positive cells (apoptotic cells) within the tumors was evaluated on 10 representative microscopic fields and the results are shown in the adjacent bar graph. Intensity of ErbB2, AKT and pAKT expression within the tumors was semiquantitative evaluated as described in Materials and Methods, and the results are shown in the adjacent bar graph (#: p=0.0015; *: p=0.04; **: p=0.0001). Scale bars correspond to 100 µm.

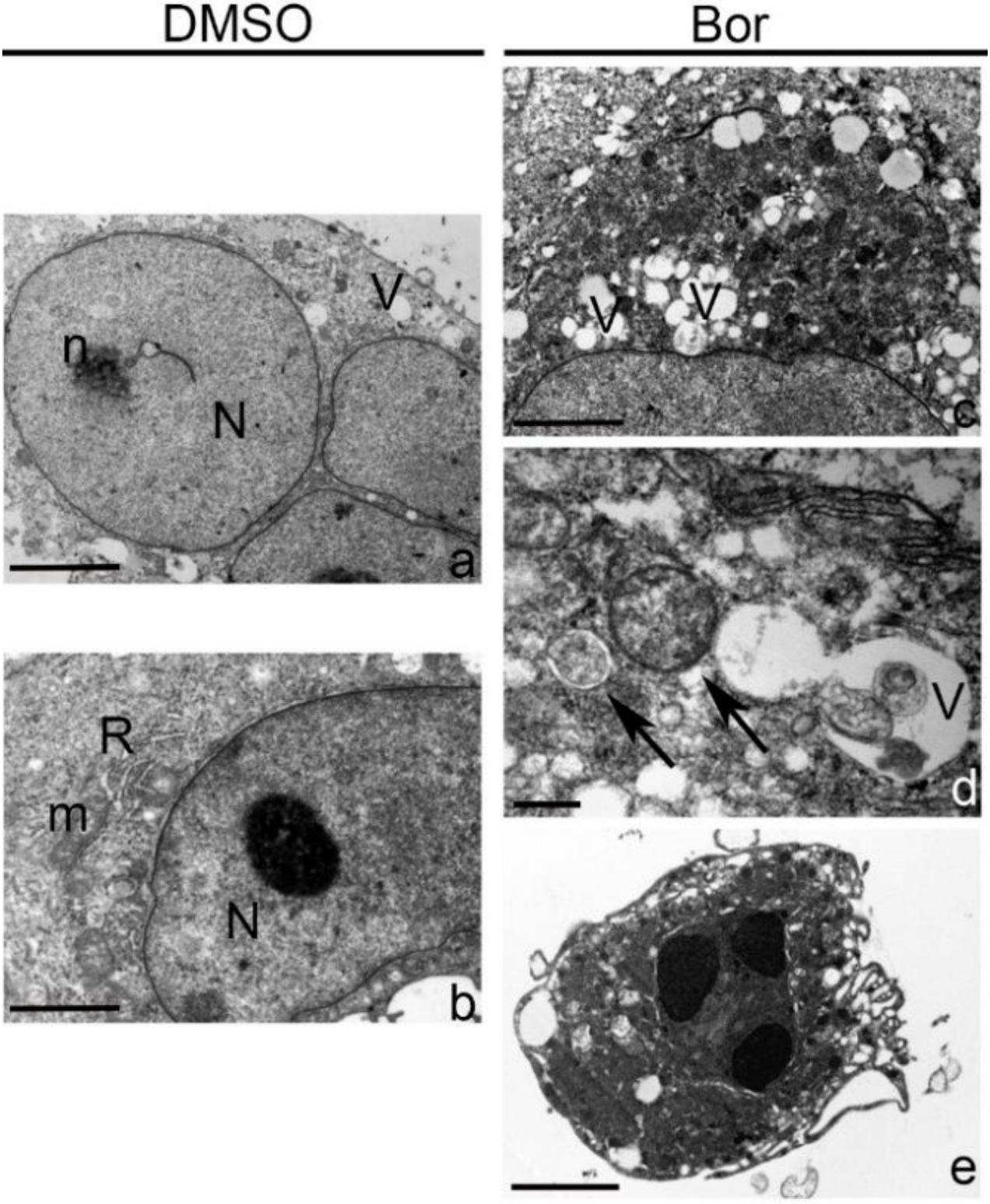

Figure 10

Ultrastructural analysis of Bortezomib- or DMSO-treated SALTO-5 cells. Ultrastructural analysis of SALTO-5 cells treated with Bortezomib (Bor) at a concentration of 25 nM (c, d, e) or with DMSO (a, b), as a vehicle control, for 24 hours. The presence of numerous vacuoles surrounded by single membrane (V) or double membrane resembling autophagosomes (arrows) in Bor-treated cells was observed. Apoptotic cells were also visible (e). N: nucleus; n: nucleolus; m: mitochondria; R: endoplasmic reticulum; V: vacuoles. Scale bars correspond to 2 μm (a,b,c,e) and 200 nm (d).

Supplementary Files

This is a list of supplementary files associated with this preprint. Click to download.

- Benvenutoetal.SupplementaryMaterial.docx